Sutrisno and Ariga *NPG Asia Materials* (2023) 15:21
https://doi.org/10.1038/s41427-023-00469-w

NPG Asia Materials

REVIEW ARTICLE Open Access

Pore-engineered nanoarchitectonics for cancer therapy

Linawati Sutrisno[1] and Katsuhiko Ariga[1,2]

Abstract

Nanoarchitectonics describes the integration of nanotechnology with other fields as a postnanotechnology concept that elevates it to material science. Based on this fundamental principle, we address pore-engineered nanoarchitectonics with application targets for cancer therapy by combining basic descriptions and exemplifying therapy applications in this review. The initial two sections briefly summarize pore-engineered nanoarchitectonics basics according to classification based on (i) material porosity and (ii) material composition. Afterward, the main application-oriented section—designing mesoporous material for cancer therapy—is presented. Various types of drug delivery systems, including mesoporous nanoparticles as nanocarriers, endogenous stimuli-responsive drug delivery, exogenous stimuli-responsive drug delivery, and targeted drug delivery, are described. Importantly, the clinical translation of mesoporous materials is further discussed. Mesoporous materials are unique nanoparticles that offer a network of cavities as vehicles for drug nanocarriers. Regarding the developments that allow mesoporous nanoparticles to be broadly used in clinical settings, there are several challenges that should be solved for their clinical application. From a clinical perspective, there are tremendous processes in the development of mesoporous materials.

Introduction

It is necessary to develop highly functional material systems to solve various social problems, such as energy, environmental, and medical issues. Many new functional materials have been developed through organic chemistry, inorganic chemistry, material chemistry, and other synthetic approaches. Clearly, the materials and the precise control of their internal structures is important for enhancing their functionality. Due to the development of nanotechnology, the specific properties and functions of nanoscale structures have been revealed. Direct observation of structures at the atomic and molecular levels has become possible[1,2], and their isolated properties have been elucidated[3,4]. However, in the field of materials science and chemistry, specific interactions between components have led to the search for manners to develop functional materials with precisely controlled structures. For example, supramolecular chemistry has been used to create materials through molecular recognition[5,6] and molecular assembly[7,8], and coordination chemistry has been used to develop porous materials with high structural regularity, such as metal–organic frameworks (MOFs)[9,10]. To make the fusions of these individual scientific fields more meaningful, it is important to integrate them into a common concept. The new concept of nanoarchitectonics will play this role[11]. Nanoarchitectonics describes the integration of nanotechnology with other fields, such as organic chemistry, polymer chemistry, supramolecular chemistry, coordination chemistry, material science, microfabrication, and biotechnology (Fig. 1)[12]. Nanoarchitectronics is a postnanotechnology concept that elevates nanotechnology to the field of material science[13].

Nanoarchitectonics is a methodology of designing functional materials using atoms, molecules, and

Correspondence: Linawati Sutrisno (SUTRISNO.Linawati@nims.go.jp) or Katsuhiko Ariga (ARIGA.Katsuhiko@nims.go.jp)
[1]World Premier International (WPI) Research Center for Materials Nanoarchitectonics (MANA), National Institute for Materials Science (NIMS), 1-1 Namiki, Tsukuba 305-0044, Japan
[2]Department of Advanced Materials Science, Graduate School of Frontier Sciences, The University of Tokyo, 5-1-5 Kahiwanoha, Kashiwa, Chiba 277-8561, Japan

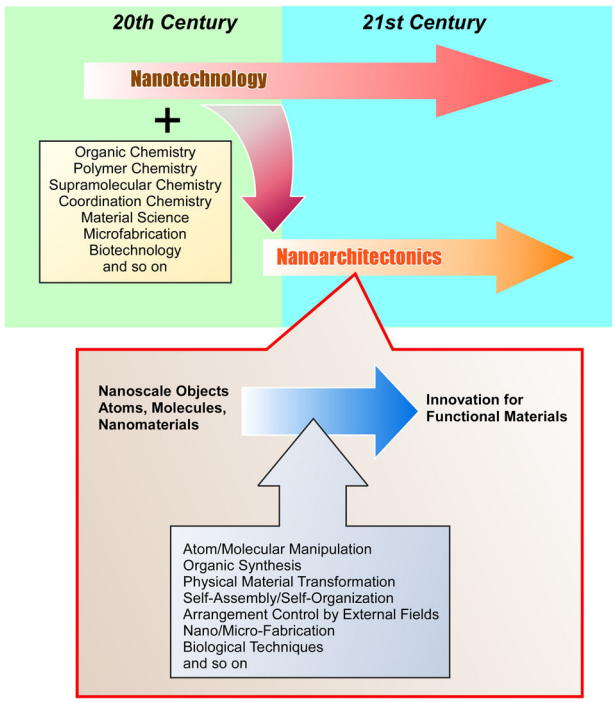

Fig. 1 Outline of nanoarchitectonics concept and methods.

nanomaterials as components. In this process, the architecture of functional materials is created by selecting and combining appropriate unit processes from atom/molecular manipulation, organic synthesis, physical material transformation, self-assembly/self-organization, arrangement control by external fields, nano/microfabrication, biological techniques, etc[14]. Different from equilibrium-based self-assembly, several processes, including nonequilibrium processes, are combined in nanoarchitectonics; this field has advantages in the fabrication of functional materials with hierarchical or asymmetric structures[15]. This concept applies without restriction to organic and inorganic materials and even biological materials. Considering that all materials are composed of atoms and molecules in principle, it is a universal concept used for all materials. Analogous to the theory of everything in physics[16], this method is called the method for everything in material science[17].

The synthesis of fine structural materials by combining several processes was practiced even before the concept of nanoarchitectonics was proposed. It is significant to address these material science concepts through nanoarchitectonics. One such example is the synthesis and architecture of porous materials, such as mesoporous materials[18,19]. For example, the synthesis of mesoporous silica is made by a combination of several processes, including self-assembly of surfactant, sol–gel reaction using it as a template, and calcination. Mesoporous carbon is made using a replica of mesoporous silica. The inner surfaces of pores in mesoporous materials can be modified with organic functional groups, complexes, and nanomaterials. Porous materials can be organized into multilayered structures. The material science of porous materials contains many elements of nanoarchitectonics. Therefore, the subject of pore-engineered nanoarchitectonics has been selected for this review.

Nanoarchitectonics is a general, substance-independent concept in which a wide range of functional material systems is architected. Accordingly, many functions and applications can be targeted. These functions have been widely used in basic science[20,21] and in applied fields, such as energy[22,23], environment[24,25], and devices[26,27]. In terms of the organization of various functional units into hierarchical structures, the products of nanoarchitectonics have something in common with biological structures. Therefore, among the many application areas, biological applications are targets where the material nanoarchitectonics express their potential. Biological applications of nanoarchitectonics have been proposed in fields ranging from fundamental, such as the organization of biomolecules[28,29], to applicable, such as the control of stem cell differentiation[30]. However, there are a few examples of its application to more practically oriented biomedical fields. Therefore, in this paper, cancer therapy is selected as the application of nanoarchitectonics.

Based on this background, this review article addresses pore-engineered nanoarchitectonics with application targets for cancer therapy by combining basic descriptions and exemplifying therapy applications. The initial two sections briefly summarize pore-engineered nanoarchitectonics basics according to classification based on (i) material porosity and (ii) material composition. Following these sections, the main application-oriented section—designing mesoporous material for cancer therapy—is presented. In this section, various types of drug delivery applications, including mesoporous nanoparticles as nanocarriers, endogenous stimuli-responsive drug delivery, exogenous stimuli-responsive drug delivery, and targeted drug delivery, are explained. Importantly, the clinical translation of mesoporous materials is further discussed. In this review, the concepts, facts, and perspectives of pore-engineered nanoarchitectonics for cancer therapy are described and discussed from basic to practical applications.

Pore-engineered nanoarchitectonics basics 1: Classification based on material porosity

According to the International Union of Pure and Applied Chemistry (IUPAC) definition, porous materials are categorized according to their pore sizes: microporous materials with pore sizes below 2 nm, mesoporous materials with pore sizes of approximately 2–50 nm, and

macroporous materials with pore sizes greater than 50 nm. One of the representative microporous materials is zeolites, which exhibit large surface areas (300–2000 $m^2 g^{-1}$) that have reached a state of maturity as catalysts and adsorbents for industrial separations[31,32]. The commercialization of zeolites has been facilitated by their high thermal stability levels, which result from their strong constituent tetrahedral bonds, such as Si–O and Al–O bonds[33]. Furthermore, the crystalline properties of zeolites provide the prediction of structures and computational screening to identify ideal architectures for certain separation applications and as their modification is applied as inracellular delively for biomedical application[34,35]. However, the small pores and low chemical stabilities of zeolites greatly limit their broad application. Therefore, various new crystalline-like materials with larger pores have been developed[36–39].

The development of mesoporous materials is inspired by the fact that microporous materials do not meet application requirements, which require effective mass transfer[40–42]. The initial report on the fabrication of the first mesoporous material (KSW-1) was written by Kuroda et al. in 1990. Mesoporous silica is created by using an intercalated complex of a layered polysilicate kanemite with alkyltrimethylammonium cationic surfactants (Cn-TMA), which has tunable pore diameters by adjusting the alkyl number of Cn-TMA. Later, ordered mesoporous silicate (MCM41) was developed by a liquid–crystal template mechanism in the presence of surfactants[43]. The materials form inorganic walls between ordered surfactant micelles, and the pore size is tuned by the intercalation of layered silicates with the addition of surfactant. In 1998, mesoporous silica SBA-15 with a pore size of approximately 300 angstroms was synthesized in acidic media using triblock copolymer as a template. The thermal stability and good repeatability of such a synthesis process have initiated the development of various mesoporous materials worldwide[44–46].

The selection of original materials and synthesis conditions has created various types of mesoporous materials. For example, neutral amine as a template is reported to produce hexagonal mesoporous silica (HMS) with disordered hexagonal architectures and thick walls. Moreover, a disordered mesoporous material (MSU-1, Michigan State University) is fabricated using poly(ethylene oxide) as a structure-directing agent[47]. Zhao et al. have reported the fabrication of highly ordered large mesoporous silica (SBA-15) by using an amphiphilic triblock copolymer of poly(ethylene oxide) and poly(propylene oxide), which results in a two-dimensional hexagonal structure and thick pore walls[48]. Later, the researchers fabricated a mesoporous material called mesocellular form (MCF), with the use of triblock copolymer-stabilized oil as templates in water microemulsions[49].

The preparation of functional mesoporous materials is a continuing research topic[50–56]. To date, general methods for synthesizing mesoporous materials have been classified into five groups: hard-templating, soft-templating,

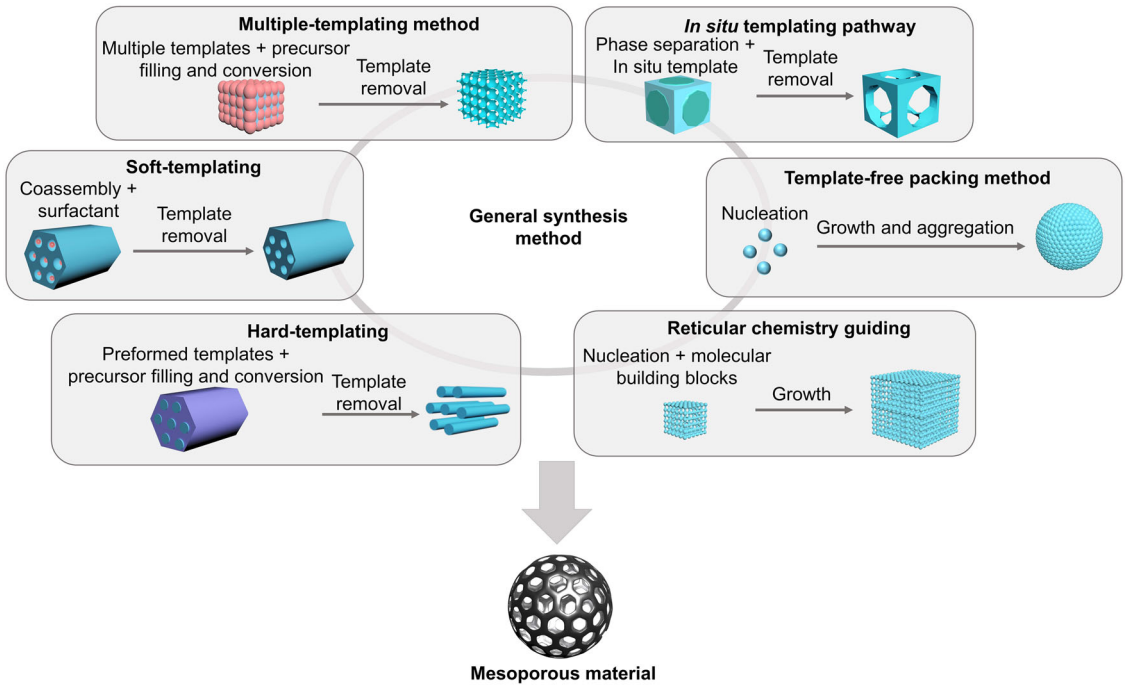

Fig. 2 Principal strategy for synthesizing mesoporous materials. There are six general methods for synthesizing mesoporous materials, including multiple-templating, in situ templating, template-free, reticular chemistry, hard, and soft templating methods.

multiple-templating, in situ-templating, template-free packing, and reticular chemistry guiding methods (Fig. 2). In the hard templating method, covalent bonds are used to retain the desired shape. The hard templating method is performed by wetting the template and depositing material into the space of the template. The soft-templating method requires surfactants, which feature hydrogen bonding and electrostatic interactions with precursors[57–59]. A combination of hard and soft-template methods generates hierarchical porous materials that have been widely explored in batteries and supercapacitors. In particular, macropores in electrodes function as reservoirs. The in situ-templating method is performed by separating the phase from chemical species in precursors during thermal or chemical treatment. The formation of mesoporous nanoparticles by a template-free strategy depends on interparticle spaces between neighboring nanoscale building blocks. In contrast to such synthetic approaches, reticular chemistry uses molecular building blocks to produce covalent–organic frameworks (COFs) or metal–organic frameworks (MOFs) with crystalline pore walls.

An understanding of the correlation between pore structure and functionality is necessary to find new methods for developing advanced porous materials. The diversity in pore size influences their permeability and selectivity for guest species. Micropore materials allow small molecules to transport and adsorb and are usually applied for gas separation and filtration, catalytic transformations, ion exchangers and absorbents. Mesoporous materials can be used as catalysts or catalyst supports in the conversion of larger molecules; they have biomedical applications in enzyme immobilization, biocatalysis, drug delivery and sensors due to their large range of sizes (2–50 nm). Macroporous materials have unique optical properties due to their porous size being comparable to optical wavelengths. Furthermore, macroporous materials are applied in the biomedical field due to their large porous sizes, such as macroporous scaffolds for the regeneration of new tissue and the growth of cells. To date, mesoporous materials have attracted significant attention in biomedical applications, especially in cancer therapy, due to their sizes, which primarily influence biodistribution after injection into the bloodstream.

Pore-engineered nanoarchitectonics basics 2: Classification according to material composition for biomedical application

A wide array of mesoporous inorganic, organic and organic–inorganic hybrid structures have been proposed for industrial, biomedical, sensor, and new energy applications[60–65]. However, in terms of the cancer field, only a few of them can be employed. The classification of mesoporous materials, which has been developed for biomedical applications based on composition, is reviewed and discussed in detail below.

Organic

Mesoporous polydopamine (PDA)

As a mussel-inspired material, mesoporous polydopamine exhibits many fascinating properties due to its high loading capacity, high biocompatibility, low cost, and high specific surface area[66–68]. In particular, engineering processes of mesoporous PDA by varying synthesis parameters aim at tunable physicochemical properties have been explored from the point of view of various practical applications. Templating methods are common methods used to prepare mesoporous PDA. For example, Zhang et al. fabricated a series of hollow magnetic mesoporous PDA with tunable pore sizes, shell thicknesses, sizes, and morphologies by adjusting the numbers of organic solvents and cotemplates (Fig. 3)[69]. First, hollow magnetic Fe_3O_4 with large cavities is synthesized via a hydrothermal method in the presence of sodium citrate as the reductant and polyacrylamide (PAMAM) as the stabilizer. Second, a PDA shell is formed based on a rapid interface-directed coassembly strategy with the addition of dual templates (F127/P123 and 1,3,5-trimethylbenzene (TMB)), ammonium hydroxide as the catalyst, anhydrous ethanol as the dispersant, and deionized water as the cosolvent. The surface structures, mesopore sizes, and morphologies are tailored by adjusting the amount of TMB. In particular, by increasing the amount of TMB in the reaction system from 0, 0.5, 1.0, 1.5, and 2.0 mL, the pore structures become more visible and regular; the morphology undergoes a process that changes the shape from uniform to inhomogeneous. Furthermore, an increase in the P123/F127 weight ratio shows a tendency to enlarge the pores of mesoporous PDA.

The controllable anisotropic growth of asymmetric and symmetric mesoporous PDA is greatly important for the development of drug encapsulation and high-performance mass transport nanosystems. Based on the considerations above, Lou et al. have reported the synthesis of bowl-like mesoporous PDA via simple emulsion-induced interface anisotropic assembly[70]. After interface formation is formed between TMB and water, composite micelles of island-shaped mesostructured PDA form at the TMB/water interface. Continuous cooperative assembly facilitates oriented growth from micelles, resulting in bowl-like mesoporous PDA with radially oriented mesopores. In brief, an emulsion solution is formed by mixing dopamine hydrochloride, TMB, and F127. Then, ammonia is added dropwise, and the product is centrifuged, redispersed in water/ethanol, and subjected to hydrothermal treatment to stabilize the structure of mesoporous PDA. By increasing the amount of TMB from 0.16, 0.18, and 0.2 mL, the morphology of mesoporous

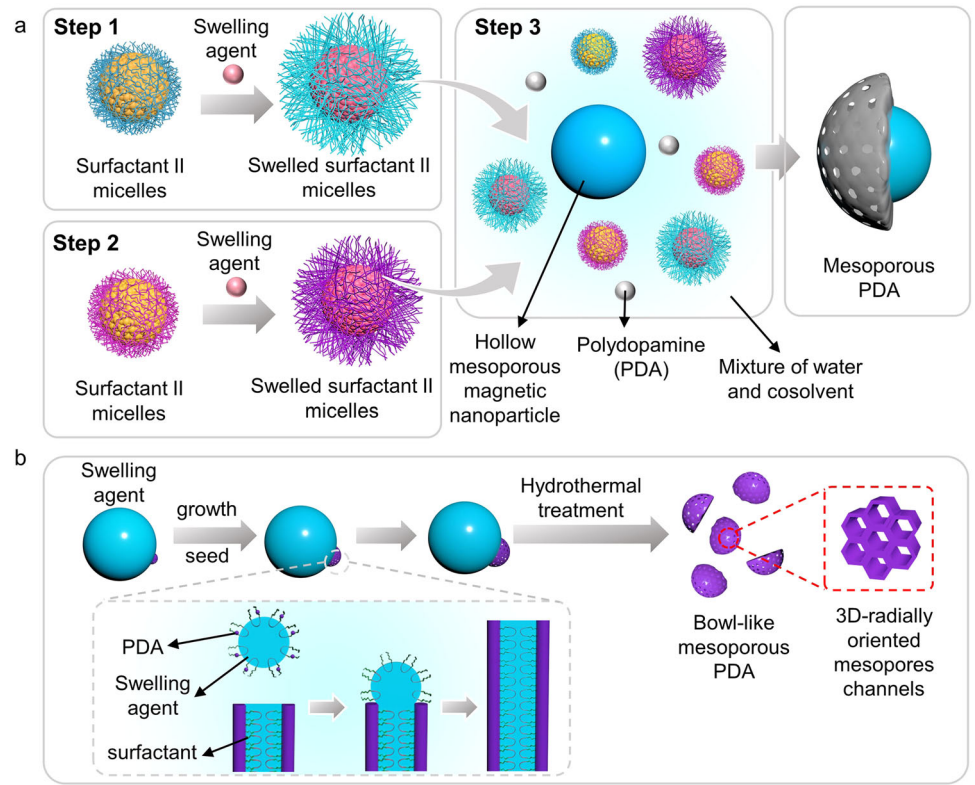

Fig. 3 Schematic diagram of the preparation of mesoporous polydopamine. a Dual surfactants as the template and (**b**) seed-growth method.

PDA is obviously changed from symmetric nanospheres to a mixture of nanospheres, bowl-like particles, and asymmetric bowl-like particles. Remarkably, without the addition of TMB or F127, aggregated solid PDA is formed. The growth of mesoporous PDA is varied by tuning the cosolvent in the reaction system. The increases in the volume fractions of cosolvents from 0, 20, 50, 60, and 80% lead to various morphologies, starting from irregular hemispherical nanoshells to round-plate, bowl-like, and asymmetric bowl-like nanoparticles. Such a phenomenon may be attributed to the fact that the presence of cosolvent slows the polymerization rate of dopamine. However, when the cosolvent concentration reaches ~60–80%, mesostructures are difficult to form, resulting in the breakage of the emulsion. When the temperature is elevated from 50–70%, the diameters of the mesoporous nanoparticles decrease relative to the reaction performed at ambient temperature. Therefore, the surfactant, cosolvent concentration, and temperature are critical factors for preparing mesoporous PDA.

In the past decade, apart from low-dimensional mesoporous architectures, complex structures of mesoporous PDA, such as core–shell, hollow, and nanosheets, have been developed for various applications[71,72]. Yamauchi et al. fabricated a sandwich-structured composite of ordered mesoporous PDA (OMPDA)/$Ti_3C_2T_x$ through in situ polymerization of dopamine on a highly conductive $Ti_3C_2T_x$ substrate[73]. In this approach, the PS-b-PEO block copolymer is employed as a soft-template, leading to vertically oriented nanopores with diameters of ~20 nm on thin films of OMPDA. Mesoporous PDA has been employed as a nanocarrier for cancer treatment. Zhao et al. synthesized core–shell mesoporous PDA-Au nanoparticles using a seed-mediated microemulsion method[74]. After preparing a stable emulsion consisting of F127, gold nanoparticles, dopamine, ammonia, and TMB in water/ethanol solution (pH 8.5), core–shell structures of mesoporous nanoparticles are obtained. Then, the nanoplatform is loaded with CRISPR–Cas9 ribonucleoprotein (RNP) and coated with polyethylene glycol–folic acid (PEG–FA). The mesoporous PDA coatings of Au cores improve the photothermal conversion efficiency of Au, facilitate targeted delivery and stimulate the release of CRISPR–Cas9 in cancer cells.

Covalent-organic framework (COF)

COF is a crystalline porous material that connects organic building blocks through thermodynamically stable covalent bonds. Various covalent bonds constructed from diverse synthetic organic reactions between different building

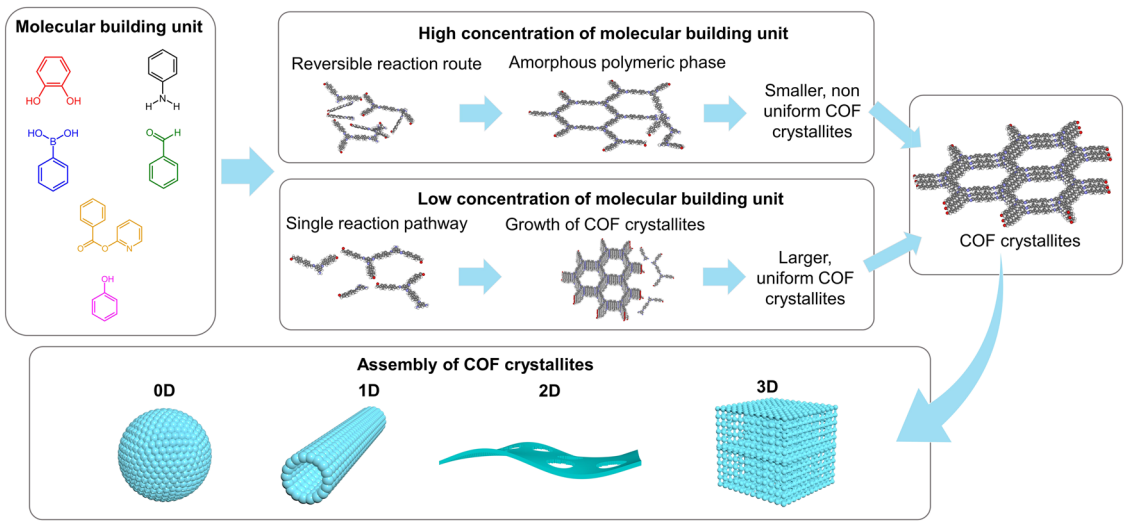

Fig. 4 Fundamental concept of the synthesis of a covalent-organic framework (COF). COF are crystalline porous materials fabricated from molecular building units that are connected through covalent bonds. By controlling the assembly of molecular building blocks, it enables the synthesis of porous structures and ability to adjust the physicochemical properties of COF.

blocks provide COFs with desirable targeted functions and crystalline structures. The steps in the synthesis of COF are divided into two major steps (Fig. 4). The first step includes the initiation of COF nuclei followed by crystal growth and COF crystallite formation. The second step is the self-assembly of COF crystallites, which is crucial for adjusting the shape, size, and different dimensionalities. The morphologeis of COFs are classified into several categories based on their dimensionalities: (1) 0D COFs (nanoparticles, nanospheres, and hollow spheres); (2) 1D COFs (nanorods, nanofibers, and nanotubes); (3) 2D COFs (thin films and nanosheets); and (4) 3D COFs (monoliths, foams, etc.)[75].

Due to their biocompatibility, tunable structures and pore sizes, COFs inherently possess tremendous potential as nanocarriers for biomedical applications[76–78]. Boron-based COFs have been widely explored as nanocarriers for various drugs; however, they suffer from hydrolytic degradation by water[79]. Hence, new types of linkages, such as hydrazone linkages, Schiff-base-type imine linkages, and covalent triazine-based frameworks, have been developed for COF-based nanocarriers[80–83]. For instance, Bhunia et al. synthesized a perylene-based COF, which acts as a reservoir for mitotoxantrone drugs. Such a nanosystem is designed based on a donor–acceptor-based strategy for albumin-triggered cellular release[84]. Bai et al. prepared 2 imide-based COFs (PI-2-COF and PI-3-COF) for the delivery of three different cancer drugs, wherein the high drug-loading capacity reaches 30% due to its large pore diameter[85]. Despite these advances, numerous COFs exhibit a lack of water solubility and poor targeting capacity. Therefore, the structure of COF is often transformed in response to various stimuli, decorated with target groups and coated with various biocompatible polymers for cancer therapy[86,87].

Inorganic

Mesoporous silica

Among mesoporous materials, mesoporous silica is most widely used for biomedical applications[88]. Conventional mesoporous silica, such as Mobil Composition of Mater (MCM-41), is produced through a soft-templating method based on sol–gel chemistry. As shown in Fig. 5a, mesoporous silica is usually prepared by mixing a silica precursor and amphiphilic surfactant to form a long-range mesoscopic periodic structure[89]. Generally, tetraethylxilane (TEOS) is utilized as a silica source and surfactant as a structure-directing template. Briefly, surfactant is dissolved and prepared as micelles under alkaline conditions. After the silica precursor is added dropwise, the surfactant adsorbs to silica via electrostatic interactions, resulting in the nucleation and condensation of mesoporous silica nanoparticles (MSNs). Finally, the surfactant template is removed to form MSNs. The steps of nucleation and growth play critical roles in adjusting the size and morphology characteristics of MSNs, while the type of surfactant affects the cavity size. For instance, MSNs produced with cetrimonium bromide (CTAB) surfactant result in pores of approximately 50 nm, while MSNs produced with pluronic and fluorocarbon surfactants have pore sizes of 5–30 nm.

To form a dual mesoporous core–shell structure, binary surfactants with different molecular weights are used[88]. Swelling agents and pore expanders, such as TMB and octane, are added to enlarge the pores of MSNs. To

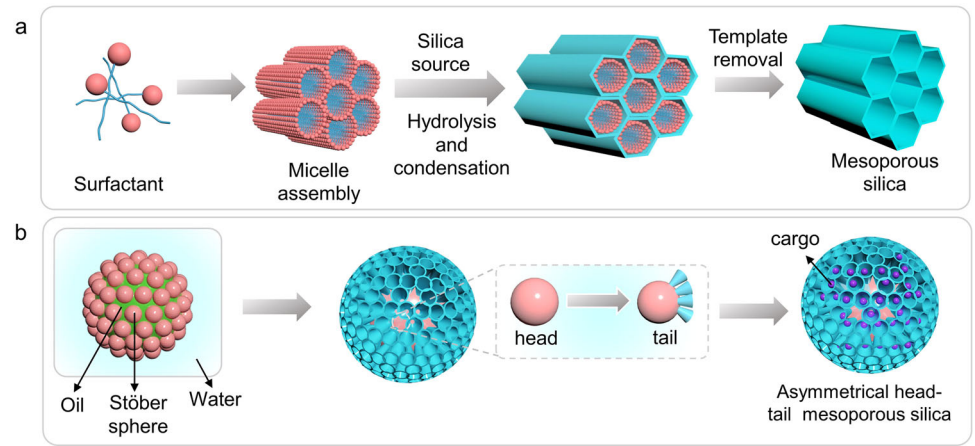

Fig. 5 Schematic illustration of the synthetic route for mesoporous silica nanoparticles (MSNs). a Typical method for the synthesis of MSNs and (**b**) Stöber method.

provide alkaline conditions during the reaction, triethanolamine and ammonia are added to the mixture solution. The alkaline pH supports highly negatively charged silica and enhances assembly and condensation through material interactions. Despite the success of using a surfactant, this process is quite complex for large-scale manufacturing. To solve this problem, a drug-structure-directing complex method has been developed to prepare MSN[90]. During this process, activated DSDAs are obtained by an amidation reaction of drugs and long hydrocarbon chain fatty acid chlorides. Next, DSDAs are reacted and self-assembled to form MSNs. Relative to traditional processes, DSDA-based MSNs have several advantages: a simplified process, enhanced payload, sustained release, and high stability.

Due to the burgeoning field of MSN applications, new demands for MSNs with various structures and performances are gradually improving. Hollow-type MSNs with mesoporous structures and interstitial hollow spaces have been developed with soft-templating, selective-etching, and self-templating; the physical parameters can be controlled by changing the synthesis conditions (pH, temperature, and solvents). Except for the pore size, various morphologies and shapes of MSNs have been developed, including cubic[91], foam-like[92], Janus-type[93,94], flower-like[95], MCM-41-like hexagonal[96], concentric[97], radial, and worm-like porosity[98]. In biomedical applications, modifications of the shape, pore structure, morphology, and silica composition highly affect the drug release kinetics after the administration of MSNs as nanocarriers to the human body. Therefore, numerous studies have been performed to analyze their behavior after administration both in vitro and in vivo. For example, He et al. reported a three-step degradation profile of MCM-41 in simulated body fluid (SBF): (1) rapid degradation after several hours, (2) decelerated degradation rate due to the presence of a calcium/magnesium silicate layer, followed by a slow diffusion stage, and (3) almost complete degradation after two weeks of immersion when the concentration of particle added is 0.5 mg mL^{-1} [99]. He et al. reported the effects of different particle sizes (80, 120, 200, and 300 nm) of PEGylated spherical MSNs on excretion in urine by intravenous administration. The smallest particle size (80 nm) shows longer blood circulation, and it easily escapes from nonspecific cell uptake in spleen, liver, and lung tissues. However, both MSNs and PEGylated MSNs have been discovered in the spleen and liver after 1 month of administration[100]. In terms of toxicity, Shi et al. reported that biodegraded products of MSNs with particle sizes of 420 nm show no obvious toxicity to either MDA-MB-468 cells or COS-7 cells[101]. Various morphologies, shell thicknesses, pore volumes, pore structures, and surface modifications provide distinct characteristics for drug delivery[102–105]. For instance, Li et al. designed persistent luminant nanoparticles (PLNPs) with MSNs as templates[106]. By controlling the pore channels of MSNs, the sizes of PLNPs are precisely tuned. PLNPs have average diameters of 2.5 and 5.0 nm and are easily metabolized through renal clearance after intravenous administration in vivo. The drug-loading capacity is highly dependent on pore size. For example, the hollow structure of MSN facilitates the drug-loading capacity becoming higher than that of the conventional MSN[107]. To improve the drug-loading capacity, many studies have attempted to produce hydrophilic and rough surfaces for enhanced physical adsorption of targeted bioactive drugs[108].

Mesoporous organosilica exhibit higher drug delivery capability than conventional MSNs due to its stable physicochemical properties and abundant active sites.

Mesoporous organosilica is synthesized from bridged organosilica precursors by a soft-templating method, where their physicochemical properties are easily modified through tunable synthesis conditions (reaction time, solvents, precursors, and temperature)[109]. Similarly, hollow mesoporous organosilica can be prepared by using the soft-template method[110]. Furthermore, their pore sizes are adjusted by varying reaction temperatures, resulting in attractive properties for applications as drug nanocarriers for cancer therapy[111].

MSNs are an ideal candidate for cancer therapy due to their excellent biocompatibility levels and easy functionalization abilities. For example, Nel et al. developed a lipid bilayer to coat MSN for codelivery of irinotecan and TLR7/8 agonist 3M-052 against cancer[112]. This work is performed by incorporating the C18 lipid tail of 3M-052 into lipid bilayer-coated MSNs. Such a lipid bilayer may reduce immune clearance for therapy against cancer, improving the efficacy of as-synthesized MSNs for cancer therapy. Dong et al. engineered pathogen-mimicking nanoparticles to stimulate reactive oxygen species (ROS) and immune responses in the tumor microenvironment[113]. MSNs are functionalized with amine groups and APTES and reacted with 4-carboxyphenylboronic, which has ROS-responsive properties. After the encapsulation of doxorubicin, it is conjugated with detoxified lipopolysaccharide (SP–LPS) through a stable cyclic ester. The as-synthesized nanoparticles show synergistic effects of chemotherapy and immunotherapy against cancer. Abbaraju et al. prepared customized head–tail structure asymmetric MSNs (HTMSNs) by the Stöber method, consisting of solid heads on dendritic tails with large pores (11–28 nm) (Fig. 5b). The asymmetric HTMSN shows low hemolysis relative to conventional MSN. After encapsulation of ovalbumine, nanodevices show a large T-cell population, which can be used as a vaccine for cancer therapy[114].

Carbon-based mesoporous materials

Mesoporous carbon usually exhibits more benefits than mesoporous silica, such as a higher surface area, larger pore size, and feasible textural properties. In general, mesoporous carbon and its derivatives are fabricated by template techniques[115]. The structure of mesoporous carbon is engineered by varying the reaction time, temperature, and solvent type. For instance, melamine, pluronic F-127, and phenolic resin copolymers are reacted and carbonized to form nitrogen-doped mesoporous carbon (N-MCNs). By varying the concentration of melamine, different nitrogen contents of N-MCNs are obtained by a one-step preparation process[116].

Fullerene, a member of the carbon family, has drawn significant attention due to its extended π-conjugation and broad applications in various fields. Although water-soluble fullerene can be fabricated, it suffers from a tendency to aggregate. Therefore, molecular nanoarchitectonics to prepare the conjugate of fullerene and other polymer chains becomes important for improving the water solubility property. For instance, Chung et al. prepared highly water-soluble fullerene with color-tunable photoluminescent properties for imaging applications. C_{60}-TEG conjugates are synthesized by the addition of lithium hydroxide as a catalyst[117]. In supramolecular polymers, the structure of fullerene is well regulated, including dendritic, linear and net-like fullerene arrays[118]. To create porosity in fullerene, a nanotemplating method is developed to prepare highly ordered mesoporous C_{60}. Vinu et al. prepared mesoporous fullerene by the addition of 1-chloronaphthalene as a solvent and mesoporous silica SBA-15 as a template. The solvent fills template pores and supports the easy polymerization of C_{60}. The mesoporous C_{60} possesses a well-ordered porous structure, rod-shaped morphology, tunable pores, and high specific surface area ($680\ m^2\ g^{-1}$)[119].

Fullerene materials and their derivatives have been developed for biorelated applications. Cell adhesion onto the substrate is highly dependent on the hydrophobicity of the scaffold surface. Since fullerene and its derivatives are hydrophobic and possess rigid mechanical properties, the use of fullerene as a scaffold for tissue engineering has been developed. For instance, Bacakova et al. reported the morphological sensitivities of human osteoblast-like MG63 cells on C_{60}-coated micropatterns. First, three-dimensional C_{60} scaffolds with different heights (130 to 1040 nm) and rectangular openings of 100 μm are prepared through vapor deposition. The results demonstrate that cells are highly localized in grooves when the height of the pattern is 1040 nm. Moreover, the patterned C_{60} might not affect cell growth[120]. Supramolecular assemblies of fullerene can be used to modify the solid surface of a scaffold. The morphology of self-assembled fullerene can be tuned from one-dimensional to three-dimensional, such as whiskers[121], tubes[122–124], sheets[125,126], cubes[127,128], and corn-husk shaped[129], using the liquid–liquid interfacial precipitation method.

Ariga et al. prepared highly aligned 1D fullerene whiskers by interfacial alignment. The orientation of myoblast cells is regulated on C_{60} nanowhisker scaffolds, while cell differentiation and proliferation are significantly promoted on C_{60} nanowhisker scaffolds[130]. A previous study reports the preparation of an aligned C_{60} nanowhisker through the vortex-Langmuir–Blodgett (v-LB) technique[119]. By simply spreading the C_{60} nanowhisker with vortex motion of the subphase, efficient alignment with various curvature geometries and packing can be obtained. Unlike the conventional LB technique, alignment geometries are controlled by altering the transfer positions from the surface to the solid surface. Parallel

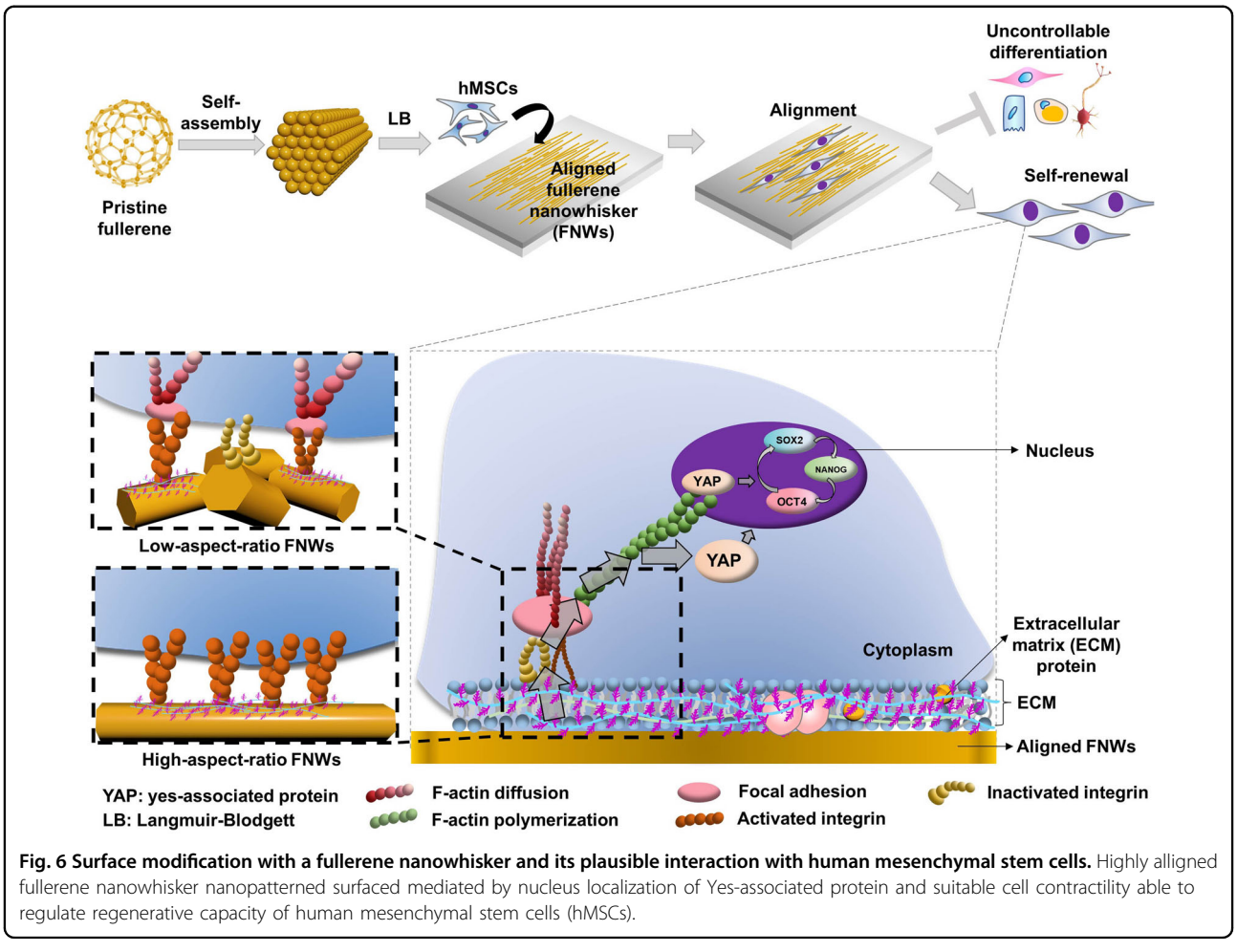

Fig. 6 Surface modification with a fullerene nanowhisker and its plausible interaction with human mesenchymal stem cells. Highly alligned fullerene nanowhisker nanopatterned surfaced mediated by nucleus localization of Yes-associated protein and suitable cell contractility able to regulate regenerative capacity of human mesenchymal stem cells (hMSCs).

aligned arrays of the C_{60} nanowhisker result from transfer, which is located far from the rotation center. Transfer at a position close to the rotation center results in curve arrays of the C_{60} nanowhisker. Human osteoblast-like MG63 cells are grown in accordance with the axes of alignment of the C_{60} nanowhisker. Neural stem cells have been reported to exhibit highly oriented morphologies after culture on highly aligned C_{60} nanowhiskers[131].

Recently, Ariga et al. used a highly aligned C_{60} nanowhisker as a scaffold to control the attachment and function of human mesenchymal stem cells (hMSCs) (Fig. 6)[132]. Continuously controllable alignments and variations in the nanoarchitectonic topographical features of fullerene nanowhiskers are obtained using the Langmuir–Blodgett technique. The appropriate YAP cell contractility and nuclear localization mediate the improvement in the long-term retention of hMSC multipotency and self-renewal on high-aligned fullerene nanowhiskers. This work offers several advantages, including excellent biocompatibility, affordable price, ease of manufacturing, tunable morphology, and maintenance of multipotency. Since the morphology of fullerene greatly influences cell growth and proliferation, fullerene-based scaffolds hold tremendous potential for tissue regeneration applications. In conclusion, mesoporous carbon-based materials have been regarded as promising materials for biological applications.

Mesoporous metal materials

Mesoporous metal oxides, such as TiO_2, Al_2O_3, CeO_2, Fe_2O_3, ZnO, Co_3O_4, WO_3, ZrO_2, and SnO_2, exhibit controllable pore structures (size, pore, volume, and types) and large surface areas, which are important for drug loading. The general synthetic strategy of mesoporous metal oxides is categorized into two types: hard template and soft-template methods (Fig. 7). Mesoporous carbon (CMK-1 and CMK-3) or mesoporous silica with different pore structures (e.g., SBA-15, SBA-16, MCM-41, MCM-48, FDU-12, and KIT-6) are often used as hard templates[133,134]. However, the complex reaction between silica and the filtrated metal ion precursor leads to the incomplete filling of mesoporous silica. Therefore, various methods have been employed to increase impregnation and decrease outside pore loading. For example,

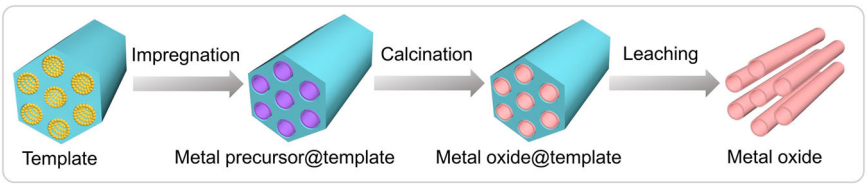

Fig. 7 General synthesis method of mesoporous metal oxides using a hard template. Hard template of mesoporous metal oxide includes three steps: impregnation of metal precursor, calcination to convert the metal into metal oxide, and leaching to obtain the mesoporous metal oxide.

mesoporous metal oxides are prepared by taking advantage of the interactions between fresh silica templates and metal ion precursors through weak Coulombic interactions. To incorporate the maximum amount of metal ion precursors, silanol is retained as much as possible. The mesoporous silica templates are functionalized by certain organic groups (such as $-NH_2$ and $-CH{=}CH_2$) to form strong interactions between the metal ion precursor and organic group[134].

Modified mesoporous metal oxides have more beneficial effects than pure mesoporous oxides, and various components are grafted onto mesoporous frameworks. The materials themselves show several beneficial effects for cancer treatment. For example, mesoporous TiO_2 exhibits excellent light absorption and generates ROS, which has a detrimental effect on cancer cells[135]. To date, numerous mesoporous metal oxides have been widely explored as nanocarriers for drug delivery or anticancer agents[136–138]. For example, Nd-sensitized UCNP@m-SiO_2@MnO_2 core–shell nanoparticles are designed for photodynamic therapy and NIR-II imaging against tumors. The loading of zinc phthalocyanine and rose bengal (RB) support the efficiency of ROS. Moreover, the manganese oxide shell shows degradability in the acidic tumor microenvironment, alleviating hypoxia and enhancing the efficacy of PDT. Importantly, biodegraded Mn^{2+} ions is applied for T1-weighted magnetic resonance imaging (MRI)[139]. The hollow cavity of mesoporous ferric oxide serves as a Fenton agent to improve chemotherapy and provides a hollow cavity for loading macrophage membrane-camouflaged carbonic anhydrase inhibitor (CAI). After internalization by tumor cells, CA IX induces the accumulation of H^+ to improve Fenton-like reactions and prevents tumor metastasis[140]. Fe_3O_4@mCuO nanospheres have been employed for the selective isolation of hemoglobin. The high magnetism of nanospheres allows easy separation by an external magnet[141]. Mesoporous metal oxides are regarded as promising candidates for biomedical applications.

Hybrid organic–inorganic: Metal–organic framework (MOF)

MOFs are fabricated through coordination interactions between metal ions or clusters and organic linkers, which results in highly porous structures. To tailor porous MOFs for biomedical applications, different metal ions and ligands are conjugated to MOFs (Fig. 8). The physicochemical properties of MOFs are regulated with the selection of linkers, metal ions, and reaction conditions (time, temperature, and pressure). Several strategies for fabricating MOFs are solvothermal, ultrasonic, microwave-assisted, and electrochemical methods[142]. In the solvothermal method, organic ligands and MOFs are reacted in closed vessels for several hours under high temperature and pressure. During the process, nucleation occurs after the concentration of reactive monomer surpasses the critical nucleation concentration; then, crystal growth and NMOF can be obtained. Ultrasonic synthesis is a method for synthesizing MOFs in which the interactions between ultrasonication and reactive liquids occurs due to the wavelengths of ultrasonic waves being larger than those of molecules. The acoustic cavitation produces a popular topic for enhancing the reactant activity. Electrochemical synthesis relies on the reaction of metal sources from the dissolution of the anode in the electrochemical cell at room temperature. Microwave-assisted synthesis is based on the interaction between mobile electric charges and electromagnetic waves in the reactant.

Due to their excellent biocompatibility and high catalytic activity, MOFs have been widely explored for biosensing, physiological catalysis, and wound healing. In the biomedical field, particle size is important for circulatory lifetime, distribution and excretion. To reduce the size of the particle, a specific growth inhibitor is usually added to delay nucleation growth[143]. Ferey et al. added iron acetate (III) to inhibit the crystal growth of porous iron muconate MOF. During crystal growth, competition between the bifunctional group carboxylate of iron muconate and the monofunctional group carboxylate of iron acetate delays the growth of nanoparticle[144]. Another strategy for controlling the sizes of MOFs is by selecting the types and ratios of solvents, surfactants, and hydrotopes. For instance, Lin et al. adjusted the molar ratio of water and surfactant to tune the size of Gd-based MOF nanoparticles[145]. The size of the MOF affects its cellular uptake and toxicity. For instance, cellular uptake of porous coordination network (PCN)-224 is in the order of 90 > 60 > 30 > 140 > 190 nm[146]. Similar to particle size, the

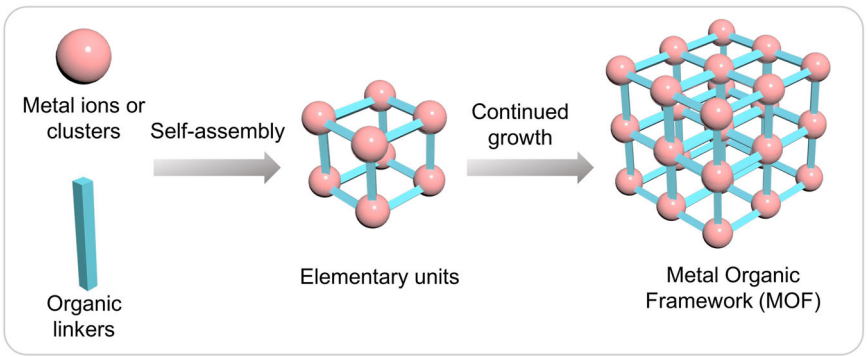

Fig. 8 General synthesis method of the metal–organic framework (MOF). Metal–organic framework are crystalline porous materials consist of a three-dimensional network of metal ions and organic ligands, forming a highly porous material with high surface area.

surface properties of MOFs greatly influence their biocompatibility. To modify the surfaces of MOFs, several modifications, such as silica shells, dendrimers, lipid bilayers, and PEGylation, have been explored[147]. Above all, a strategy for modifying MOFs for cancer therapies is a promising direction for inhibiting the rate of tumor proliferation.

Designing mesoporous materials for cancer therapy

Mesoporous nanoparticles as nanocarriers

The modifiable properties of mesoporous nanoparticles make them ideal nanocarriers for drug delivery applications. Numerous studies have focused on the development of mesoporous nanoparticles to release various anticancer and imaging agents. Ideally, a drug delivery system must control the release profile and specifically direct it to a specific cell or tissue. To improve the capacities of mesoporous nanoparticles to transport payloads to targeting tissues, many great efforts have been made to construct them with responsiveness to single or multiple physicochemical triggers. The stimuli-responsive drug release minimizes their adverse effects on healthy organs and increases drug efficacy. In this section, we summarize recent advances in mesoporous nanoparticles in the drug delivery area and discuss the underlying nanoarchitectonics of mesoporous nanoparticle-based nanoplatforms for biomedical applications. According to the type of trigger release, mesoporous nanoarchitectures can be categorized as endogenous-triggered nanoarchitectures and exogenous-triggered nanoarchitectures. Both passive and active targeting are summarized in this section (Fig. 9).

Endogenous stimuli-responsive drug delivery

Cancer cells metabolize in distinct pathways relative to healthy cells due to the disruption of mutation oncogenes and tumor suppressor genes. Mutated metabolic enzymes lead to malignant transformation, which affects cell growth, proliferation, and endogenous variations in biochemicals in the tumor microenvironment[148,149]. The distinct characteristics of cancer cells have been widely explored to trigger drug release for precise cancer treatment with mitigated adverse effects. Such a strategy has been used to design feasible mesoporous nanoarchitectures for tumor-specific treatment[150].

Response to pH

The intensified aerobic glycolysis of cancer cells—the Warburg effect—results in copious H^+ and the overproduction of lactate in tumor microenvironments[151,152]. This phenomenon initiates the local downregulation of extracellular pH in cancer cells, which is approximately 6.7–7.1[153]. Many anticancer drug delivery systems take advantage of the pH differences between healthy tissues (~7.4) and solid tumors (6.7–7.1). Hence, effective pH-responsive nanoarchitectures must provide a sharp response to a change in pH in the tumor surrounding microenvironment. The pH values of different cell compartments and organelles are different. For example, the pH of mitochondria, cytosol, Golgi apparatus, endosomes and lysosomes are ~8.0, 7.4, 6.4, 5.5 and 5.0, respectively[87]. Therefore, pH-responsive mesoporous nanoparticles can be designed based on the differences between pH values and their targets to promote cell internalization.

Several mesoporous nanoparticles themselves have pH-responsive properties. For example, Du et al. constructed gated channel-interconnected mesoporous carbon for stimuli-responsive controlled release of drugs[154]. Carboxylated mesoporous carbon is covalently attached to carboxylated ZnO quantum dots via dual amide linkages. Since ZnO has pH-responsive properties, the sustained release of drugs is activated upon reduction in pH. The cancer-responsive property results in high biocompatibility toward normal cells while achieving high anticancer efficacy at low pH values. Various pH-sensitive polymers

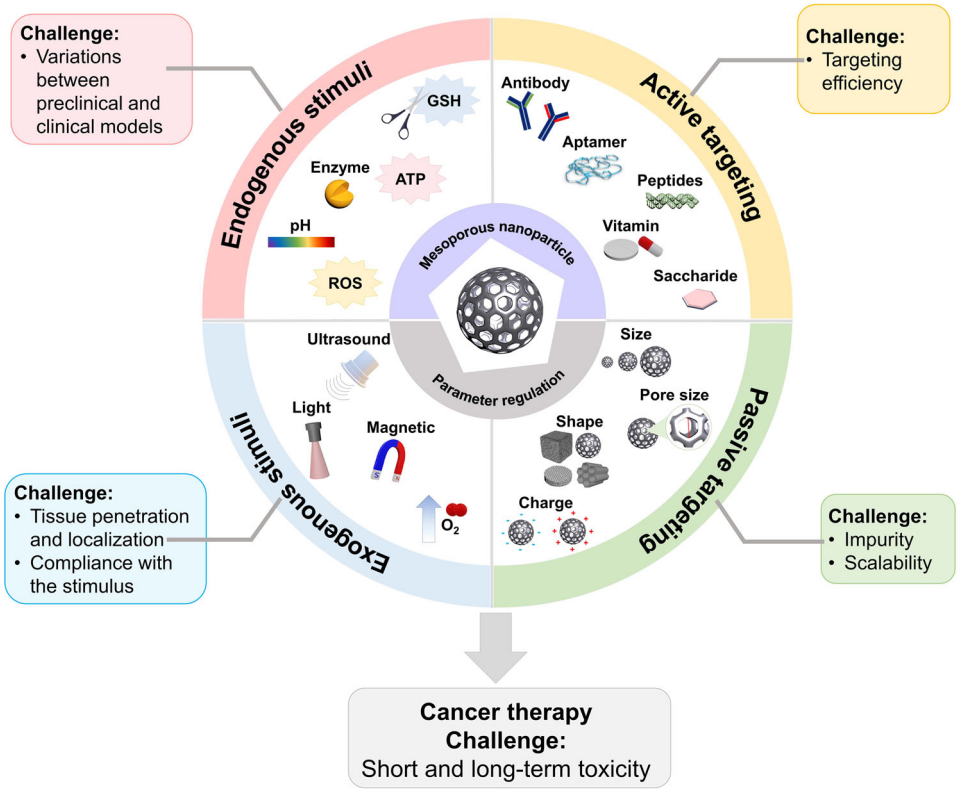

Fig. 9 Design considerations for engineering mesoporous nanoparticles for cancer therapy. Stimuli-responsive mesoporous nanoparticles improve the specificity of drug delivery in tumor microenvironments or inside cancer cells for on-demand drug accumulation and delivery. To effectively improve its potential use in the clinical trials, there are several challenges that should be taken into considerations, such as targeting efficiency, impurity, scalability, short and long-term toxicity, tissue penetration, variation between cellular, preclinical, and clinical model.

have been grafted to the surfaces of mesoporous nanoparticles and serve as pH-responsive shells. Examples of pH-sensitive materials to modify mesoporous nanoparticles are chitosan[155], gelatin[156], polymeric lipids[157,158], poly(2-(diethylamino)ethylmethacrylate, poly(4-vinyl pyridine)[159], starch, polystyrene, poly(2-(dimethylamino) ethylacrylate[160], coordination polymers[161], ferritin[162], and poly(allylamine hydrochloride)[163]. Yang et al. coated MSNs with biocompatible pH-responsive materials, including bis-aminated poly(glycerol methacrylate)s and cucurbit[7] uril, through a layer-by-layer method (Fig. 10a)[164]. The nonspecific adherence of lipids and serum proteins often forms a protein corona that induces the mistargeting of nanoparticles. Some mesoporous nanoparticles are engineered with charge reversal properties to overcome this problem. For this reason, Zhao et al. reported the codelivery of the 2,3-dioxygenase (IDO) inhibitor 1-methyltryptophan and glucose oxidase (GOx) using a MOF-based nanoplatform for tumor starvation/oxidation immunotherapy (Fig. 10b). The MOF nanoparticle is synthesized through covalent crosslinking with ROS-responsive agents and Mn^{2+}, which can easily degrade in the presence of ROS. The pH-responsive compound that is conjugated onto the modified MOF, and GOx and IDO inhibitor are loaded onto the nanosystem. Before arrival at the tumor site, the nanosystem has a negative charge, mitigating noncellular uptake by normal cells. Upon arrival at the tumor site, the size is decreased, and the nanosystem has a negative charge, leading to a shielding shell and triggering the release of drugs against cancer. The reduction in size allows nanoparticles to penetrate deep tissue[165].

Alternatively, the presence of acid-sensitive bonds enables the release of anticancer drugs. Examples of pH-sensitive linkages are hydrazone, imine, oxime, amide, acetals and orthoesters[166]. For example, Xian et al. designed and prepared a series of two-dimensional imine-linked COFs by orthogonal combination via a condensation reaction by using 1,3,5-tris(4-aminophenyl) benzene (TAPB)/TAPT and TFTPA/5,5,5-(1,3,5-benzenetriyl) tris[2-pyridinecarboxaldehyde] (BTPA) as building linkers. By varying the monomer, various pKa values of COF are obtained. All COFs show pH-dependent fluorescence relative to their building blocks, which can be used for cancer imaging due to their reversible protonation and deprotonation characteristics.

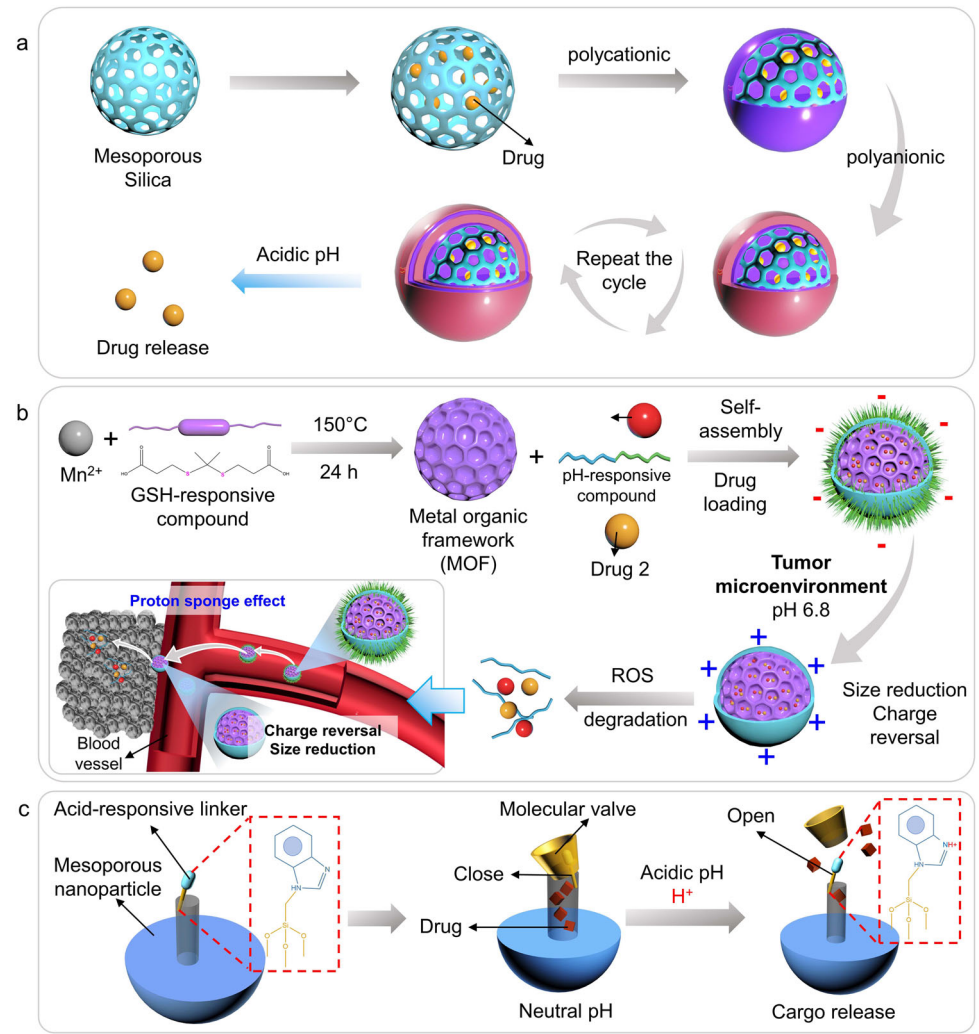

Fig. 10 Modification of mesoporous nanoparticles to achieve the pH-triggered release of cargo. a Layer-by-layer assembly. **b** Size shrinkage and charge reversal triggered by the acidic tumor microenvironment. **c** pH-responsive gatekeepers consisting of stalks and nanovalves on mesoporous nanoparticles.

Mesoporous nanoparticles have been modified based on supramolecular nanovalves to tightly close at physiological pH (~7.4) values and open at acidic pH (~6.0) values (Fig. 10c)[167]. First, the MSN surface is attached to positively charged ammonium groups by the cocondensation method. The *N*-methylbenzimidazole stalk is attached to β-CD, and then dye and drug molecules are loaded into MSN. Deprotonation at pH levels below 6 dissociates β-CD caps and enhances the release of molecules. These works demonstrate that a pH-responsive therapeutic approach contributes to the development of precision cancer therapy in the future.

Redox-responsive

Oxidative stress is an emerging hallmark of the tumor surrounding microenvironment, and cancer cells adapt by amplifying the antioxidant system. The concentration of the ROS detoxifying system (e.g., glutathione (GSH)) is elevated significantly to neutralize excess ROS[168,169]. Previous research has reported that GSH levels in tumor tissues are 4-fold higher than those in healthy tissue in mice[170]. Therefore, strategies for designing GSH-responsive nanoarchitectures have been widely explored to improve therapeutic efficacy.

The degradation rate under GSH conditions is highly dependent on the physicochemical properties of mesoporous nanoparticles (Fig. 11a). Therefore, by modulating physicochemical properties (size, porosity, condensation degree, and surface functionalization), the selectivity levels of mesoporous nanoparticles after administration are improved[99,171]. For instance, Moghaddam et al. reported that the degradation profiles of mesoporous

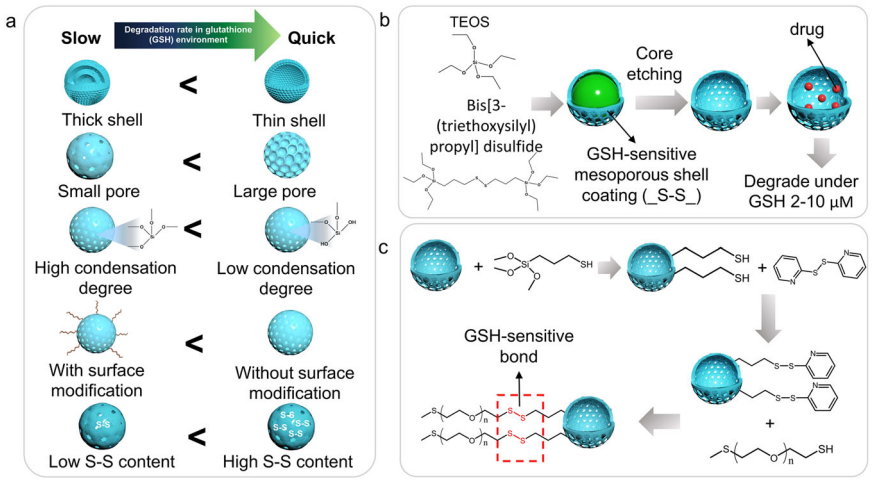

Fig. 11 Overview of the design of mesoporous nanoparticles used in the glutathione (GSH) environment. a Comparison of the degradation rate in mesoporous silica nanoparticles; (**b**) modification based on core–shell nanoparticles; and (**c**) conjugation with GSH-sensitive bonds.

organosilica are greatly influenced by both the composition and porosity of the core[172]. The nonporous nanoparticles undergo surface erosion, while porous nanoparticles undergo both bulk and surface erosion in the presence of GSH (8 mM). Chen et al. reported a comparison of the degradation profile between mesoporous organosilica and MSNs in simulated body fluid solutions with different GSH concentrations[111]. Mesoporous organosilica is degraded into fragments after incubation for 7 days in a GSH environment, while MSNs show only slight degradation in the presence of GSH.

The mesoporous nanoparticle is usually modified to serve as glutathione peroxidase for GSH depletion by conjugating different linkages or by coating using a GSH-sensitive mesoporous shell[173]. Generally, these chemicals exhibit excellent biocompatibility and many functional groups, improving the stability of drugs via strong bonding effects in a low GSH environment. After arrival at the GSH environment, these gates trigger the release of cargo based on the breakage of chemical bonds. For instance, Ghandehari et al. prepared a GSH-responsive hollow MSN-based selective-etching technique, anchored disulfide linkages in the outer shell of hMSNs and loaded doxorubicin into hMSNs (Fig. 11b). First, MSNs are synthesized through the hard-template method. Second, a disulfide-based mesoporous shell is coated onto the core with two precursors: TEOS and bis[3-(triethoxysilyl)propyl] disulfide. Finally, a selective-etching method is performed using a high concentration of sodium carbonate as the etching agent, and anticancer drugs are loaded onto mesoporous nanoparticles. In vitro results show that hMSNs accumulated in endolysosomes of MCF-7 cells and are nontoxic to MCF-7 cells within a concentration range of 0–1000 μg mL^{-1} [174]. Similarly, Wu et al. integrated hollow mesoporous organosilica (HMON) capsules with ultrasmall $Cu_{2-x}Se$ via disulfide bonds and loaded doxorubicin into nanoarchitectures (Fig. 11c)[175]. In this study, we focus on the breakage of disulfide bonds and the ultrasound-facilitated delivery of doxorubicin into brain cancer. The on-demand release of doxorubicin shows the significant inhibition of brain cancer cell growth while maintaining high biocompatibility, further demonstrating the high feasibility of nanoarchitectures for glioblastoma treatment. Excessive ROS is a distinct feature of the tumor microenvironment, and ROS-responsive nanoarchitecture is a promising method for developing effective cancer therapy[176,177]. Several studies have combined strategies to deplete GSH and increase ROS concentrations to improve anticancer efficacy. For instance, Fe_3O_4 nanoparticles and CB-839 are integrated into Mn-etched dendritic MSNs to promote synergistic peroxidase treatment and dual GSH depletion properties. The dendritic MSN structure is etched by the breakage of Mn, and it triggers the release of Fe_3O_4, Mn, and CB-839 in a tumor microenvironment. Subsequently, the Fenton-like activity of Fe^{2+} and Mn^{2+} catalyze H_2O_2 into highly toxic radicals in acidic environments. The released Mn^{4+}/Mn^{3+}/Fe^{3+} results in GSH oxidation and induces ferroptosis. This synergistic approach is expected to contribute to the development of cancer therapeutics.

Protein-responsive

Elevated expression levels of proteins (e.g., MMP-2 and MMP-9) have frequently been developed as triggering signals for cancer therapy[178,179]. The MMP-2-activated shrinkable nanoarchitecture is constructed for the precise delivery of anticancer drugs[180]. Briefly, paclitaxel and Ce6 are encapsulated into amine-modified MSNs. Then,

aPDL1 is conjugated via a maleimide linker, and cross-linked gelatin is selected as the outer layer of the nanoarchitecture. The gelatin layer effectively degrades after the addition of MMP2, and the size of the nanoarchitecture decreases, facilitating tumor penetration and cellular uptake in the tumor microenvironment. Such nanoarchitecture holds great potential for drug delivery systems based on mesoporous nanoparticles.

Exogenous stimuli-responsive drug delivery

Although endogenously triggered nanoarchitectures have shown promising modalities to treat cancer, complicated tumor microenvironments suffer from a lack of maneuverability. This phenomenon may be because these endogenous reactions are uncontrolled and occur spontaneously. Therefore, facile and rational design by using exogenous intervention is desirable to control the release of drugs because it may enable switching on and off on demand[181,182].

Light responsive

Light-responsive biomaterials are very attractive for triggering drug release from mesoporous nanoparticles. First, the degree of stimulation is tuned by adjusting the intensity or time of light exposure. Second, cell-material interactions are easily controlled by using a specific wavelength range. Third, light has low toxicity and a more precise cancer region site for controlling biomaterials relative to variations in pH or temperature[183]. Different light interacts with biological tissues in different manners. Once entering living tissues, light is reflected, absorbed, or scattered. In general, longer wavelengths of light exhibit lower energy levels, reducing the reaction activity with biological tissues. The strong interactions between visible light and biological tissue cause strong autofluorescence, high toxicity, and shallow penetration depth. Since NIR light has a low wavelength and low energy, it results in less tissue scattering and low absorption in biological tissues. In addition, the NIR window has deep penetration and low toxicity to cells[184,185].

In terms of cancer therapy, NIR can be applied for photothermal, photodynamic, or nanocarrier applications for light-triggered drug release[186–188]. In photothermal therapy, NIR light interacts with several materials to produce heat to induce cell death. Qu et al. developed monodispersed mesoporous antimony (Sb) nanospheres via a selective-etching route with tunable pores for photothermal therapy against cancer (Fig. 12a)[189]. To control the shape, dodecylthiol (DDT) and oleylamine are used as capping ligands, while octadecene, $SbCl_3$, and tert-butylamine borane are chosen as the solvent, semimetal precursor, and reductant, respectively. After chemical reduction, Sb nuclei are formed, oxidized, and grown. Finally, a selective-etching process is performed by reacting with DDT to form mesopores. The pore size of mesoporous Sb is tailored by adjusting the oxidative degrees of Sb nuclei. During the photothermal process, the increase in temperature promotes the dissolution of Sb nanocrystals in aqueous solution, which is positively correlated with the pore sizes of the mesopores. Such unique properties boosts the release efficiencies of nanocarriers for various types of anticancer drugs, resulting in good anticancer efficacy. Jiang et al. encapsulated carfilzomib (CFZ) into hollow titanium nitride (TiN) against tumor lymphatic metastasis (Fig. 12b)[190]. Due to the superior plasmonic property of TiN, the material exhibits excellent photothermal properties in the NIR II region. Therefore, the TiN nanoshell acts as a nanocarrier for carfilzomib and presents combined chemo-phototherapy against cancer cells.

Photodynamic therapy damages tissue because of cytotoxic species generated by photosensitizers. During photodynamic therapy, photons are absorbed and transferred to oxygen to produce ROS. Recently, two-dimensional nanoscale MOFs emerged as a new class of photosensitizers. Two-dimensional nanoscale MOFs have been reported to be able to elevate the frequency between oxygen and photosensitizers and to induce the diffusion of singlet oxygen, thus enhancing photodynamic therapy. In vivo results show that Hf-5,15-di-p-benzoatoporphyrin nMOFs exhibit a high cure rate, high tumor inhibition rate, and low metastasis potential[191]. A previous study reports a synergistic approach of photodynamic and photothermal therapy. For instance, indocyanine green and the PFKFB3 kinase inhibitor 3-(3-pyridyl)-1-(4-pyridynyl)-2-propen-1-one (3PO)-loaded (SPMI/3) are loaded into sialic acid-PEG-modified mesoporous dopamine nanoparticles to inhibit tumor metastasis and normalize tumor vasculature[192]. Typically, SPMI/3 shows antitumor properties due to the combination of photodynamic and photothermal therapy under laser irradiation. Photodynamic therapy induces the slow release of 3PO from SPMI/3, which results in normalized tumor vasculature. This finding provides an effective approach for improving photodynamic therapy via the normalization of tumor vessels.

Ultrasound responsive

The heat generated by ultrasound is used to design thermosensitive capping systems for mesoporous nanoparticles as nanocarriers, while mechanical effects are used to uncap pores. The advantages of using ultrasound-responsive materials are that they are easily tuned by adjusting the power density, exposure time, duty cycle, and frequency values. The frequency of ultrasound changes the potential cavitation and penetration depth. Moreover, potential cavitation and thermal effects affect the intensity of ultrasound. When a focused ultrasound

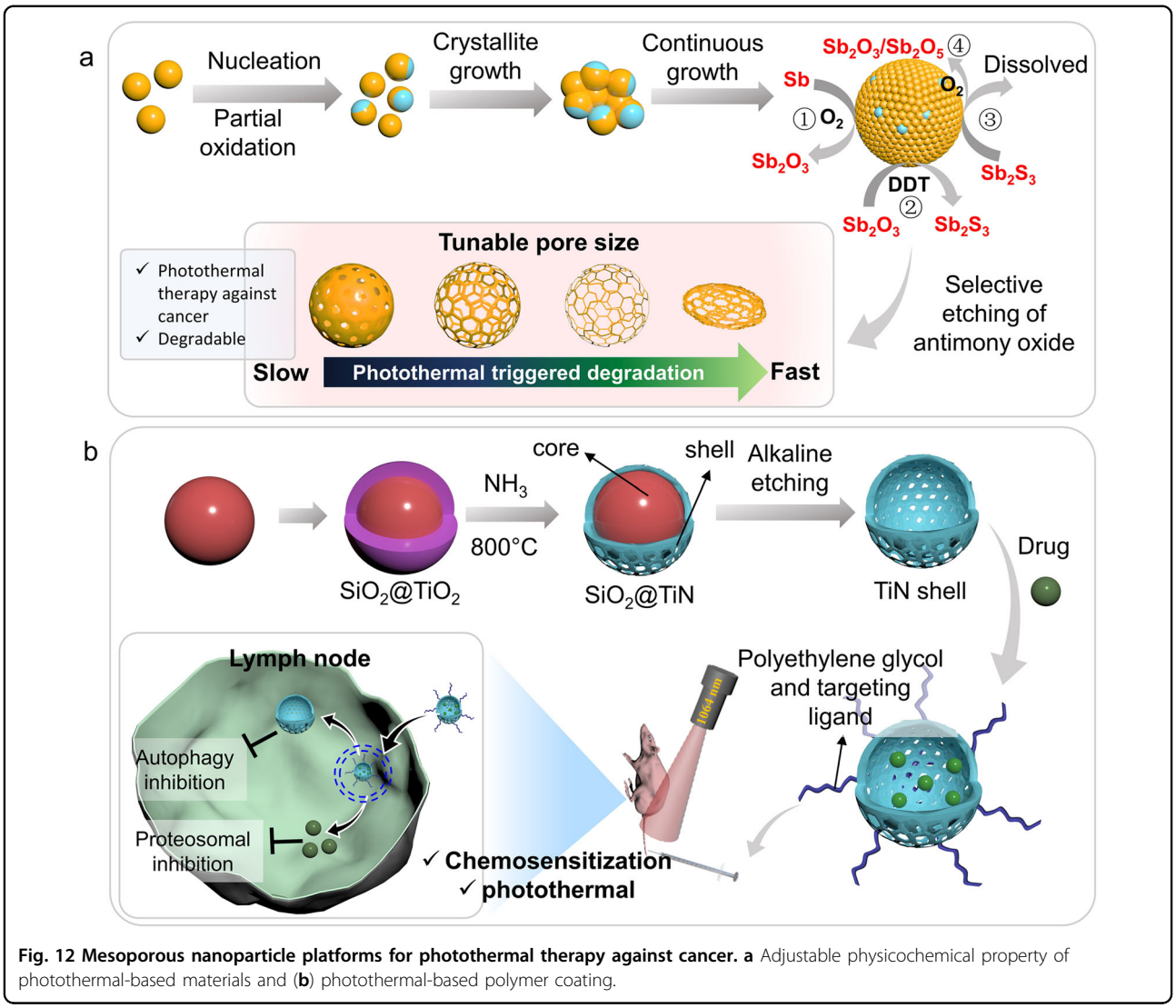

Fig. 12 Mesoporous nanoparticle platforms for photothermal therapy against cancer. a Adjustable physicochemical property of photothermal-based materials and (**b**) photothermal-based polymer coating.

beam is applied to a fixed location in a small volume, irradiation with high-intensity acoustic energy occurs and generates heat[193]. High-intensity focused ultrasound (HIFU) triggers the release of drugs at a targeted site while mitigating side effects. HIFU shows minimal invasiveness, disrupts the blood–brain barrier (BBB) and has been applied for cancer therapy[194]. For instance, doxorubicin and phase transformable perfluoropentane (PFP) are encapsulated into hollow mesoporous organosilica nanoparticles[195]. Afterward, macrophages (RAW 264.7 cells) are internalized, resulting in cell bombs. After reaching the tumor site, a short pulse of HIFU facilitates the production of large microbubbles and releases the drug from the cells. Another study has fabricated a multifunctional nanovaccine consisting of L-arginine (LA) encapsulated into black mesoporous titania (BMT)[196]. L-arginine acts as an exogenous supply of nitric oxide, and BMT serves as an acoustic sensitizer. Ultrasound stimulates the release of BMT and LA to generate singlet oxygen and nitric oxide, inducing the apoptosis of cancer cells. By combining sonodynamic/gas/immunotherapy with the injection of an anti-PD-L1 antibody, the synergistic effect of sonodynamic/gas/immunotherapy results in a strong antitumor response. Another strategy for modifying mesoporous nanoparticles for ultrasound-responsive therapy has been developed by Qiao et al. by coating MSNs with ultrasound-responsive polymers to form ultrasound-responsive nanogels (Fig. 13)[197]. Such approaches hold promise for cancer theranostic purposes.

Magnetic-responsive

The magnetic field shows advantages of deep penetration relative to light and ultrasound. Alternating magnetic fields (AMFs) have been widely explored in various biomedical areas, such as magnetic resonance imaging, nanocarriers, and hyperthermia. For instance, MSN has

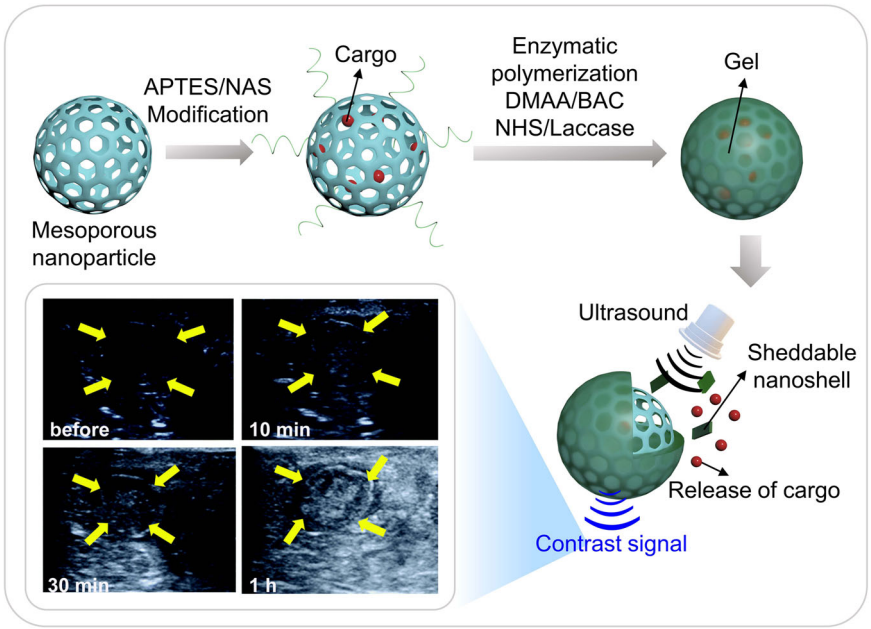

Fig. 13 Mesoporous nanoparticle-based ultrasound-responsive delivery system for drug delivery. Adapted with permission from [197], copyright 2016 Royal Society of Chemistry.

been designed by incorporating superparamagnetic iron oxide and lanthanide-ion-doped mesoporous tin oxide upconversion nanoparticle[198]. The modified mesoporous nanoparticle is further conjugated with poly(ethylene) glycol and phosphorylated serine to improve solubility and biocompatibility. Under magnetic stimuli, nanoarchitectures relieve hypoxia, enhance oxygen levels, and enhance the photodynamic effect against tumors. In a similar approach, a nanoarchitecture of superparamagnetic iron oxide ($MnFe_2O_4$@$CoFe_2O_4$) in a mesoporous silica shell is fabricated to control drug release by AMF exposure[199]. By tuning the AMF time, C–N bonds cleave, displace caps, and trigger the release of the drug from MSNs. A previous study has developed magnetic manganese oxide sweetgum-ball nanospheres (MMOSs) as nanocarriers for cancer treatment[200]. MMOSs are composed of mesoporous manganese oxide nanosheets, which are assembled on magnetic iron oxides. The nanoarchitecture is prepared based on the coprecipitation method, and the sample is collected by magnetic decantation. The mesopore structures of MMOSs are loaded with doxorubicin and chlorin e6 (Ce6), thereby showing chemo-photodynamic therapy under a magnetic field.

Cloaking techniques allow mesoporous nanoparticles to avoid clearance systems and instability during circulation. To improve the robustness of mesoporous nanoparticles, natural red blood cell membranes (RBCs) or lipid bilayers have been employed to coat MSNs (Fig. 14)[112,201]. Li et al. coated MSNs with magnetic colloids, cargo, and RBCs for cancer therapy. Briefly, after the fabrication of MSNs by a sol–gel process, magnetic nanoparticles and anticancer drugs are attached to the surfaces of the MSNs. Finally, an RBC membrane is constructed on the surfaces of the as-prepared MSNs. Such a magnetic-responsive nanoarchitecture presents unique feasibility for cancer therapy in the future.

Targeted drug delivery

Passive targeting

Passive targeting through the enhanced permeation effect (EPR) in cancer is developed from the quick proliferation of solid tumors, which results in the formation of blood vessels to provide oxygen and nutrients for further tumor growth. Such an environment leads to relatively poor lymphatic drainage and a slow excretion rate. By taking advantage of this phenomenon, several parameters for the synthesis of mesoporous materials have been adjusted to improve their selectivity to be delivered at the tumor site (Fig. 15)[202]. For example, hollow and spherical MSNs are preferred for biomedical applications due to the high surface area, large void space and low density for therapeutic cargo[203]. Short-rod MSNs (aspect ratio of 1.5) easily accumulate in the liver, while long-rod MSNs (aspect ratio of 5) are easily trapped in the spleen. The shapes of mesoporous materials greatly impact cell uptake, cell viability, apoptosis, adhesion, migration, cytoskeleton, and elimination in the human body. The short-rod MSNs have a faster clearance rate than the long-rod MSNs. Long-rod MSNs are reported to be

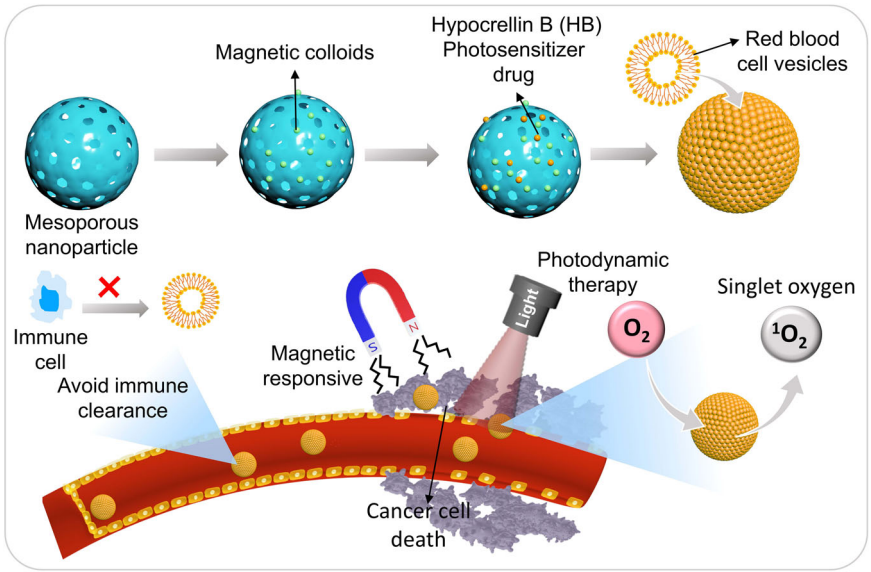

Fig. 14 Strategy for avoiding the immune clearance of magnetic-responsive mesoporous nanoparticles. Integral membrane proteins in red blood cell membranes act as self-markers, which avoid immune clearance and extend blood circulation.

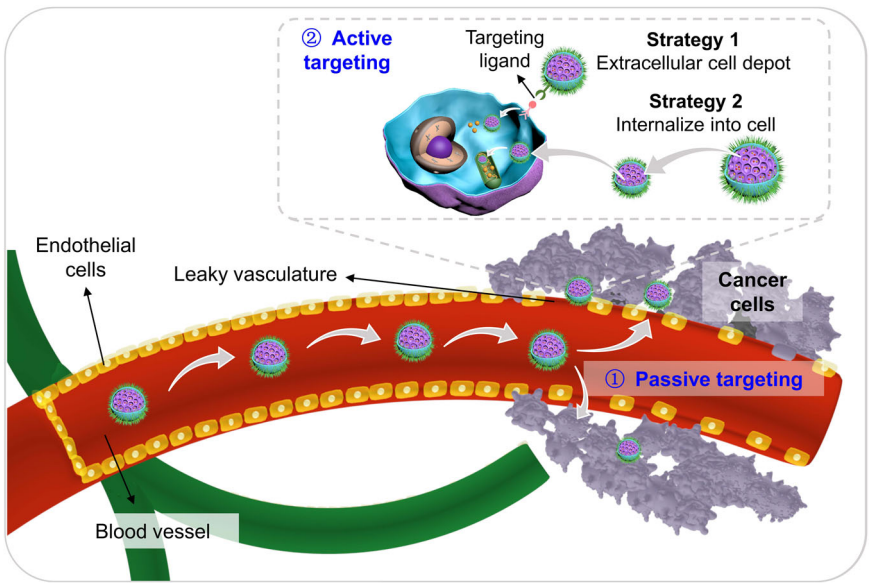

Fig. 15 General uptake pathways of passive and active targeting, which ultimately determine mesoporous fate after administration. Passive targeting takes advantage of enhance permeation effect and abnormal tumor physiology. In passive drug delivery system, nanoparticles can be modified by modifying their size, shape, and surface charge. Active targeting inroduces targeting moiety onto the nanoparticle system to improve specificity in cancer cells, both extracellular and intracellular.

internalized in large amounts and to have fast internalization rates. Surface charges determine the interactions between nanoparticles and their interactions with cell uptake and negatively charged cell membranes[204]. Regarding cell uptake, positively charged nanoparticles show higher cell uptake than negatively charged nanoparticles.

The size and geometry characteristics of mesoporous nanoparticles have been reported to impact their interaction with various biological barriers and the cancer microenvironment. For cancer application, particle size must be less than 400 nm to guarantee transport within the vascular system and easy elimination from the body[205]. Moreover, to obtain high accumulation in tumor

sites, nanoparticle diameters should be designed below the cutoff sizes of tumor vessels. Since tumor vessels range from 200 nm to 1.2 μm, a diameter of 200 nm is favorable for specific tumor accumulation[206,207]. By considering this fact, Kim et al. designed nanoparticle-loaded nanoparticles based on the intracellular and extracellular pH values of tumors[208]. The nanoarchitecture is prepared by the synthesis of MSNs (diameter ~150 nm, pore size ~15 nm), in which small Au nanoparticles (size ~15 nm) are loaded by DNA hybridization. After systemic administration, nanoarchitectures accumulate in the tumor region via the EPR effect. Subsequently, the low acidic pH (~6.5) in the tumor microenvironment results in the first transition of DNA and dissociated Au due to their small size. After the internalization of Au into tumor cells, the second DNA transition releases the anticancer drug at endosomal pH (~5.0). Such a nanoarchitecture accumulates in tumor sites through leaky vascular structures, allows Au NP diffusion to tumor tissues, and releases drugs under acidic pH. This drug delivery system is a feasible and rational design because large outer nanoparticles are important in blood circulation and allow small nanoparticles to penetrate deeply into tumors.

Active targeting

Although passive targeting is a promising modality to achieve high accumulation at the tumor site, it is still not effective enough for cancer therapy. Active targeting is developed as a supportive strategy for enhancing tumor localization once passive targeting is completed[209]. In active targeting, specific cancer targeting ligands are conjugated to the surface of mesoporous nanoparticles to allow them to interact with intracellular or extracellular cancer cells (Fig. 15). There are two cellular targets in which mesoporous nanoparticles are directed via active targeting methods: cancer cell targeting and tumoral endothelium. Cancer targeting ligands include cell organelle targeting, cell membrane targeting, and multitargeting. The different targeting moieties include antibodies[210,211], aptamers[212], peptides[213], saccharides[214], proteins[215] and vitamins[216]. For example, a previous study has conjugated antiHER2/neu mAb on the surfaces of MSNs to target breast cancer cells[217]. Such nanoarchitectures enter cells through receptor-mediated endocytosis and escape to the cytosol. Wang et al. prepared dual-responsive chiral mesoporous silica nanorods by grafting phenylboronic acid pinacol ester (PBAP) onto amino-functionalized nanorods[218]. Then, doxorubicin is incorporated into mesoporous nanoparticles, and the nanoarchitectures are coated with cyclodextrin-modified hyaluronic acid. Hyaluronic acid functions as a tumor-targeting ligand that can target CD44 receptors. Folic acid has been explored for targeting folate receptors on the surfaces of various cancer cells[219]. For example, MSN is functionalized with siloxane-cored polyamidoamine (PAMAM) dendrimer and folic acid to target the folate receptor of MCF-7 cells (Fig. 16)[220]. In another example, the TAT peptide is reported to be capable of targeting the nuclear pore complex and binding import receptors to facilitate MSN entry into the nuclei of MCF-7/ADR cancer cells[221]. Furthermore, peptides have been extensively employed as promising cancer theranostic treatments. Peptide-based mesoporous nanoparticles exhibit two advantages. First, the nanoparticles allow higher structural stabilities than their individual drug molecules. Second, the peptide-based mesoporous nanoparticle provides favorable cancer therapeutic effects, such as desired pharmacokinetics and improvement in selectivity[222]. For example, synthetic nanochaperone for peptide (SNCP) based on mesoporous silica nanoparticles are fabricated to mediate the apoptosis of cancer cells. After the immobilization of p53pep, the stabilization structure of the p53 peptide is induced from a random-coil structure to an α-helical structure[223].

Clinical translation of mesoporous materials

Although numerous passively targeted strategies have been developed for many years, it is still difficult to have advanced past clinical trials due to the challenges of biological barriers, such as high toxicity, lack of selectivity, clearance by the immune system, undesirable pharmacokinetic profile, and endothelial barriers (Fig. 17). In this section, we summarize clinical trials that have been performed on mesoporous nanoparticles, which attempt to investigate their biomedical application.

MSN has been regarded as safe by the US FDA, used as food additive E551, and it is in phase I and phase II clinical trials. The oral administration of MSNs shows minimal adverse effects while enhancing the pharmacokinetic properties of hydrophobic drugs. As depicted in Fig. 18, the biosafety of silica in the clinic has been proven in many clinical trials and two clinical studies. In phase I human studies, ibuprofen is encapsulated into a silica nanoparticle-lipid hybrid formulation. After a single oral dose is administered in 16 healthy male adults, bioavailability is increased by 3.5-fold relative to the reference fenofibrate formulation Lipanthyl[224]. MSNs have been explored for the reduction in atherosclerosis and cardiovascular disease-related death by modifying them with iron oxide and gold (NCT01270139)[225,226]. Further studies are conducted by modifying MSNs with Au shells for the thermal ablation of prostate cancer (NCT02680535, NCT04656678 and NCT04240639) and head and neck cancer (NCT00848042)[227,228]. The pilot clinical study with 16 patients diagnosed with prostate cancer indicates excellent photothermal ablation using Au shell–silica nanoparticles while minimizing their side effects.

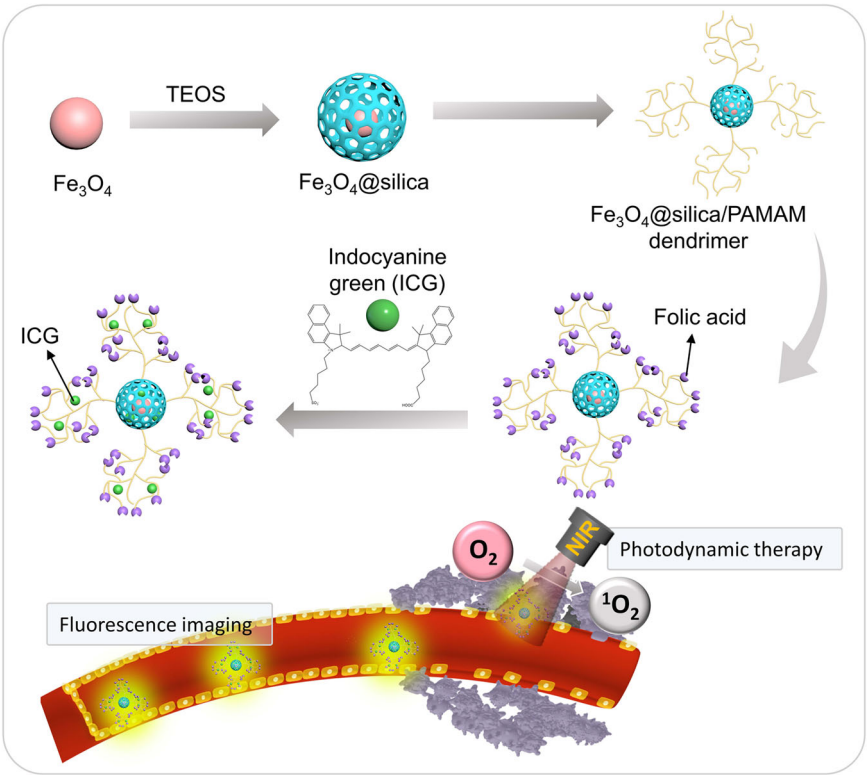

Fig. 16 Modification of dendrimer-functionalized mesoporous nanoparticles based on an active targeting strategy. Addition of targeting moieties such as folic acid to the mesoporous nanoparticle improves the specificity to tumor site, leading to the high antitumor efficacy.

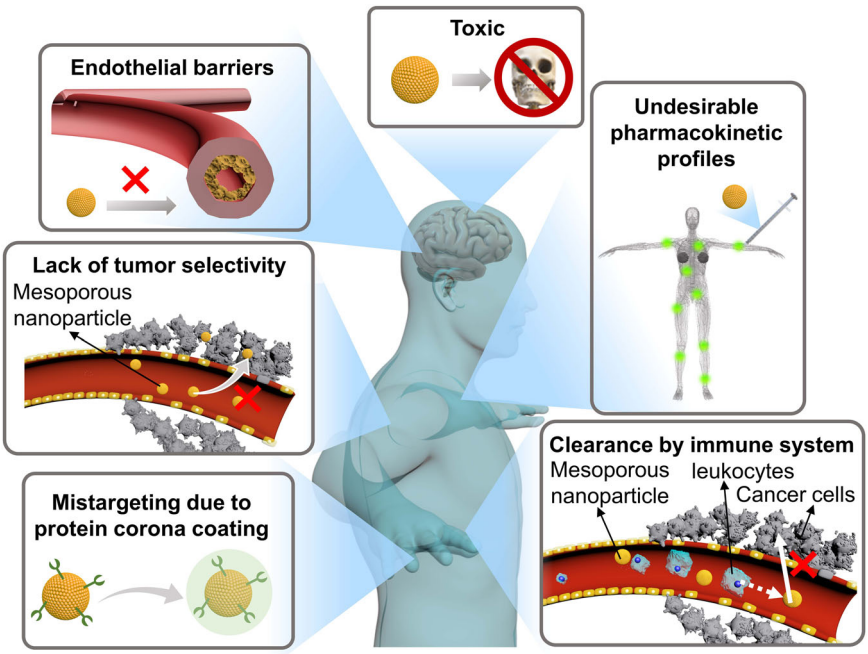

Fig. 17 Biological barriers of injectable mesoporous nanoparticles in practical applications. The main biological barriers are endothelial bariers, toxicity, undesirable pharmakokinetic profles, rapid clearance by immune system, mistargeting due to protein corona coating, and lack of tumor selectivity.

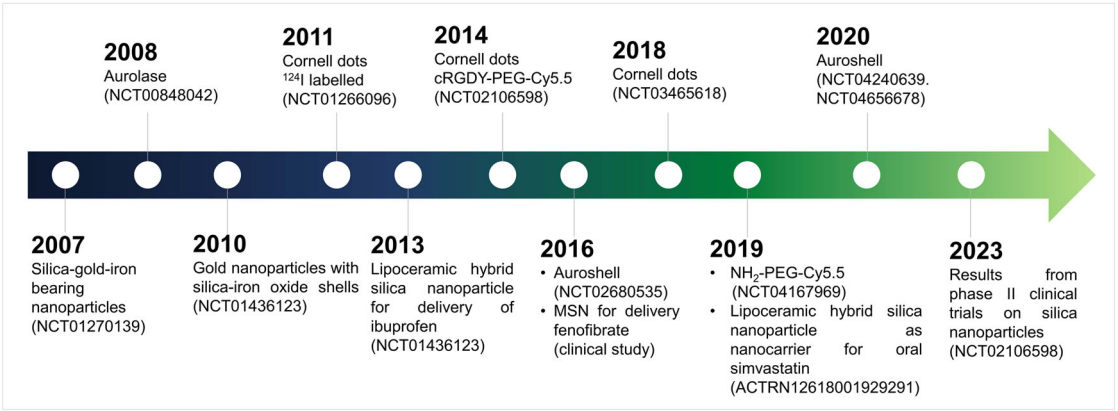

Fig. 18 Timeline of mesoporous silica nanoparticle (MSN) development in clinical trials. The timeline displays different types of MSN and the development in clinical trials. cRGDY cyclic arginyl-glycl[1]aspartic acid-tyrosine, PEG polyethylene glycol.

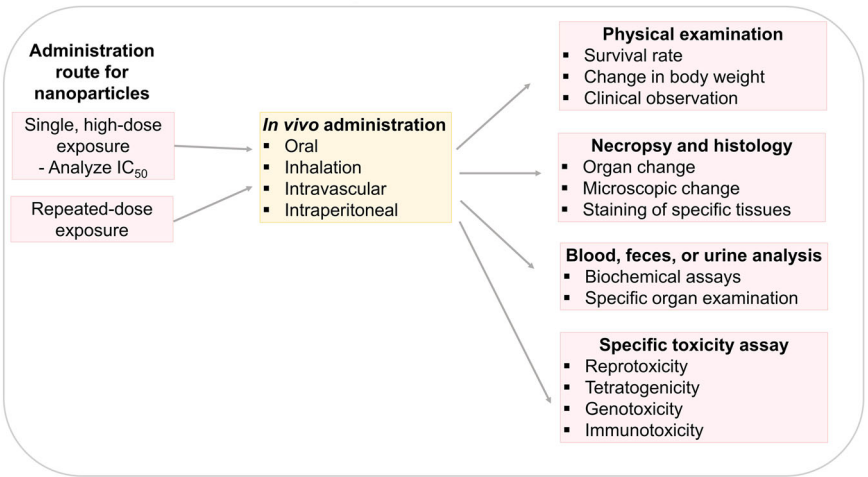

Fig. 19 Schematic diagram of the toxicology assay in vivo. After in vivo administration of nanoparticles with the certain dose, the toxicity of nanoparticles can be assessed from physical examination, change in tissues, pharmakokinetic change, and specific toxicity assay.

Cornell dot-silica encased fluorescent nanoparticles have been applied as tumor tracers due to their rapid kidney clearance. Cornell dots functionalized with cyclic arginine–glycine–aspartic acid–tyrosine peptides (cRGDY-PEG-Cy5.5-nanoparticles) have been used as tracers of various tumors, including melanoma and brain tumors (NCT01266096, NCT02106598, and NCT03465618)[229]. Cornell dots have been used in human trials for their applications in positron emission tomography imaging and tumor staging, such as brain cancer and melanoma (NCT01266096)[230]. Cornell dots are reported to be stable in the in vivo microenvironment with a half-life of ~8.7 h. The clearance and biodegradability of mesoporous nanoarchitectures are important prerequisites for clinical translation. These two factors have become major concerns since most mesoporous materials accumulate in the human body and induce adverse effects. Mesoporous silicon (Bio-Silicon) has been developed as a vehicle for intratumoral delivery. BioSilicon can be micronized, and its size can be tuned to specifically target cancer and achieve the desired biodegradability and biocompatibility[231]. The degradation property of Si can be adjusted by tuning the surface oxidation, surface functionalization, size, morphology, and porosity. For instance, surface-oxidized or silica-coated silicon NPs maintain their stabilities for up to 12 and 40 h, respectively. Nanoneedles or discoidal morphology have been reported to be stable for a few days. Different types of oxide doping onto silica and the pH of the surrounding microenvironment affect the degradation time in the human body. In terms of clearance, dextran-coated porous silicon is excreted 1 day postinjection. Silica quantum dots are easily cleared in several days, while MSNs remain in the

human body for several weeks. The excretion rates of positively charged particles are faster than those of negatively charged nanoparticles. The tunable properties of MSNs indicate tremendous potential for cancer therapy with high specificity and minimal adverse effects.

Despite the safety of clinical translation, the process of silica nanoparticles entering clinical application remains slow. For instance, it takes approximately two decades for gold shell–silica nanoparticles to enter clinical trials. This phenomenon may be due to the complexity of in vivo toxicology studies and the process of entering clinical trials, which are expensive and time-consuming (Fig. 19). Silica exhibits several advantages relative to organic nanoparticles: by altering their physicochemical and structural properties, such as charge, size, and shape, silica nanoparticles transport drugs across biological barriers. In the case of silica synthesized from Stöber nanoparticles, toxicity is found with decreasing size in mice. When administered intravenously, 300 nm nanoparticles show nontoxic properties at 200 mg kg^{-1}. However, 70 nm is reported lethal at 45 mg kg^{-1}, and 30 nm is lethal at 12 mg kg^{-1} in mice. In human clinical trials, small 10 nm nanoparticles and nanoparticles with sizes of 60–70 nm and 90–150 nm are reported to be safe after intravenous injection at 20 mg kg^{-1}. Moreover, the long-term intraperitoneal injection of MSNs with sizes of 100–130 nm (50 mg kg^{-1}) twice a week show no toxicity[232]. Despite having suitable size, shape, and degradability, high purity during synthesis is crucial for improving the biocompatibility of MSN[233]. Therefore, MSNs with high stability, synthesis method, and biocompatibility are emerging as promising nanocarriers in the development of nanoformulation.

Limitations of current studies

Mesoporous nanoparticles have potential for enhancing the stability and solubility characteristics of various drugs and blood circulation times, generating excellent results in a cellular and preclinical model[234]. However, the number of nanoparticles available to patients is far below projections for fields due to the translational gap between preclinical and clinical studies. Such a gap comes from a lack of understanding of differences in biological matrices between animals and humans, which greatly affects the behavior and functionality of nanoparticles in the body. For instance, only a few studies have focused on the effects of as-synthesized mesoporous nanoparticles on the immune system, inflammatory reactions, and complex biological matrices. In addition, compliance to stimuli and immunotoxicity, including genotoxicity to immune cells, cell dysfunction, and long-term toxicity, are rarely investigated. Furthermore, recent studies lack a focus on comparing the administration routes of nanoparticles, endotoxin contamination, and the influences of sterility on the proinflammatory effect.

The differences across preclinical and clinical studies are factors that limit success in practical applications. Heterogeneity between patients is one of the major problems of failure in nanomedicines, and there is very little research on the interactions between mesoporous nanoparticles in stratified patient populations. As a consequence, very few approved nanomedicines are applied as first-line treatments. Other reasons for the failure of mesoporous applications in clinical trials are complex manufacturing processes, low stability during storage, poor repeatability, low percent yield, and impurities in the synthesis of mesoporous nanoparticles. The presence of impurities, such as metal ions or surfactants, may affect toxicity evaluation. Considering the facts above, a simple procedure, percentage of impurities, improvement of stability during storage, and percent yield of nanoparticles should be considered when tailoring the precision design of nanomedicine.

Conclusion and future perspectives

Over the past several decades, hierarchically porous materials with various pore structures and compositions have been prepared using many strategies. As delineated, the tunable porosity, large surface area, adjustable chemical composition, and abundant surface chemistry make mesoporous nanoparticles highly promising nanoarchitectures for various cancer therapies. In this review, we have summarized the recent development of mesoporous materials. Mesoporous materials can be prepared from organic, inorganic, and organic–inorganic materials. Recent advances in mesoporous materials for cancer therapy have been comprehensively elucidated, and design strategies have been discussed in depth. Mesoporous material is a unique nanoparticle that offers a network of cavities as a vehicle for drug nanocarriers. Regarding the necessary methods for allowing mesoporous nanoparticles to be broadly used in clinical settings, there are several challenges that they should be fulfilled. Mesoporous materials should meet suitable biocompatibility, biodistribution, stability, and biodegradability characteristics. From a clinical perspective, there are tremendous processes in the development of mesoporous materials. However, a large amount of work still needs to be performed before these materials can be broadly used in clinical applications.

In addition to clinical demonstration, future prospects still require a scientific approach based on the concept of nanoarchitectonics. In material fabrication by nanoarchitectonics, it is advantageous to fabricate multicomponent structures. Moreover, it is proposed that a system similar to that of living organisms can be constructed in which these components work in harmony in the presence of thermal fluctuations[235]. Therefore, it should be possible to fabricate porous materials with a homogeneous structure consisting of a few components, as has been demonstrated thus far, to fabricate porous materials with

complex elements and to perform advanced treatment using these materials. In the past, it has not always been easy to design and build such complex systems. However, the introduction of materials informatics, which has made remarkable progress in recent years, is expected to make it possible to design complex systems. A fusion of nanoarchitectonics and materials informatics for porous materials has actually been proposed[236]. Although the recently proposed functional targets are limited in the fields of catalysis and energy, they may include medical fields, such as cancer treatment. Methodological development through the introduction of new conceptual innovations, advanced fields, and realistic clinical research is important for the development of this field.

Acknowledgements
This study was partially supported by JSPS KAKENHI Grant Numbers JP20H00392, JP20H00316 and JP21H04685.

Author contributions
L.S.: conceptualization, methodology, and writing—original draft. K.A.: supervision, writing—review and editing, and project administration.

Competing interests
The authors declare no competing interests.

Received: 28 August 2022 Revised: 15 February 2023 Accepted: 17 February 2023.
Published online: 31 March 2023

References

1. Sugimoto, Y. et al. Chemical identification of individual surface atoms by atomic force microscopy. *Nature* **446**, 64–67 (2007).
2. Bacilla, A. C. C. et al. Triangular expanded hemiporphyrazines: Electronic structures and nanoscale characterization of their adlayers on Au(111). *Bull. Chem. Soc. Jpn.* **94**, 34–43 (2021).
3. Kimura, K. et al. Selective triplet exciton formation in a single molecule. *Nature* **570**, 210–213 (2019).
4. Kazuma, E. Real-space studies of plasmon-induced dissociation reactions with an STM. *Bull. Chem. Soc. Jpn.* **93**, 1552–1557 (2020).
5. Ariga, K. Molecular recognition at the air–water interface: nanoarchitectonic design and physicochemical understanding. *Phys. Chem. Chem. Phys.* **22**, 24856–24869 (2020).
6. Harada, A., Takashima, Y., Hashidzume, A. & Yamaguchi, H. Supramolecular polymers and materials formed by host-guest interactions. *Bull. Chem. Soc. Jpn.* **94**, 2381–2389 (2021).
7. Datta, S. et al. Self-assembled poly-catenanes from supramolecular toroidal building blocks. *Nature* **583**, 400–405 (2020).
8. Percec, V. & Xiao, Q. Helical self-organizations and emerging functions in architectures, biological and synthetic macromolecules. *Bull. Chem. Soc. Jpn.* **94**, 900–928 (2021).
9. Hosono, N. Design of porous coordination materials with dynamic properties. *Bull. Chem. Soc. Jpn.* **94**, 60–69 (2021).
10. Liu, C. et al. In situ growth of three-dimensional MXene/metal–organic framework composites for high-performance supercapacitors. *Angew. Chem. Int. Ed.* **61**, e202116282 (2022).
11. Ariga, K., Ji, Q., Hill, J. P., Bando, Y. & Aono, M. Forming nanomaterials as layered functional structures toward materials nanoarchitectonics. *NPG Asia Mater.* **4**, e17 (2012).
12. Ariga, K., Ji, Q., Nakanishi, W., Hill, J. P. & Aono, M. Nanoarchitectonics: a new materials horizon for nanotechnology. *Mater. Horiz.* **2**, 406–413 (2015).
13. Ariga, K. Nanoarchitectonics: what's coming next after nanotechnology? *Nanoscale Horiz.* **6**, 364–378 (2021).
14. Ariga, K., Li, J., Fei, J., Ji, Q. & Hill, J. P. Nanoarchitectonics for dynamic functional materials from atomic-/molecular-level manipulation to macroscopic action. *Adv. Mater.* **28**, 1251–1286 (2016).
15. Ariga, K. et al. Nanoarchitectonics beyond self-assembly: Challenges to create bio-like hierarchic organization. *Angew. Chem. Int. Ed.* **59**, 15424–15446 (2020).
16. Laughlin, R. B. & Pines, D. The theory of everything. *Proc. Natl Acad. Sci.* **97**, 28–31 (2000).
17. Ariga, K. & Fakhrullin, R. Materials nanoarchitectonics from atom to living cell:A method for everything. *Bull. Chem. Soc. Jpn.* **95**, 774–795 (2022).
18. Kankala, R. K. et al. Nanoarchitectured structure and surface biofunctionality of mesoporous silica nanoparticles. *Adv. Mater.* **32**, 1907035 (2020).
19. Maji, S. et al. Macaroni fullerene crystals-derived mesoporous carbon tubes as a high-rate performance supercapacitor electrode material. *Bull. Chem. Soc. Jpn.* **94**, 1502–1509 (2021).
20. Ariga, K., Mori, T., Kitao, T. & Uemura, T. Supramolecular chiral nanoarchitectonics. *Adv. Mater.* **32**, 1905657 (2020).
21. Ariga, K. & Shionoya, M. Nanoarchitectonics for coordination asymmetry and related chemistry. *Bull. Chem. Soc. Jpn.* **94**, 839–859 (2021).
22. Kim, J., Kim, J. H. & Ariga, K. Redox-active polymers for energy storage nanoarchitectonics. *Joule* **1**, 739–768 (2017).
23. Liu, X. et al. Nanoarchitectonics of MXene/semiconductor heterojunctions toward artificial photosynthesis via photocatalytic CO_2 reduction. *Coord. Chem. Rev.* **459**, 214440 (2022).
24. Pham, T.-A. et al. Nanoarchitectonics for wide bandgap semiconductor nanowires: Toward the next generation of nanoelectromechanical systems for environmental monitoring. *Adv. Sci.* **7**, 2001294 (2020).
25. Boukhalfa, N., Darder, M., Boutahala, M., Aranda, P. & Eduardo Ruiz-Hitzky, E. Composite nanoarchitectonics: Alginate beads encapsulating sepiolite/magnetite/Prussian blue for removal of cesium ions from water. *Bull. Chem. Soc. Jpn.* **94**, 122–132 (2021).
26. Ariga, K., Ito, M., Mori, T., Watanabe, S. & Takeya, J. Atom/molecular nanoarchitectonics for devices and related applications. *Nano Today* **28**, 100762 (2019).
27. Ariga, K., Lvov, Y. & Decher, G. There is still plenty of room for layer-by-layer assembly for constructing nanoarchitectonics-based materials and devices. *Phys. Chem. Chem. Phys.* **24**, 4097–4115 (2022).
28. Liang, X., Li, L., Tang, J., Komiyama, M. & Ariga, K. Dynamism of supramolecular DNA/RNA nanoarchitectonics: From interlocked structures to molecular machines. *Bull. Chem. Soc. Jpn.* **93**, 581–603 (2020).
29. Shen, X., Song, J., Sevencan, C., Leong, D. T. & Ariga, K. Bio-interactive nanoarchitectonics with two-dimensional materials and environments. *Sci. Technol. Adv. Mater.* **23**, 199–224 (2022).
30. Hu, W., Shi, J., Lv, W., Jia, X. & Ariga, K. Regulation of stem cell fate and function by using bioactive materials with nanoarchitectonics for regenerative medicine. *Sci. Technol. Adv. Mater.* **23**, 393–412 (2022).
31. Lan, K. & Zhao, D. Functional ordered mesoporous materials: present and future. *Nano Lett.* **22**, 3177–3179 (2022).
32. Davis, M. E. Zeolites from a materials chemistry perspective. *Chem. Mater.* **26**, 239–245 (2014).
33. Liu, Y. et al. Design and synthesis of a zeolitic organic framework. *Angew. Chem. Int. Ed.* **61**, 24 (2022).
34. Lee, J.-S. M. & Cooper, A. I. Advances in conjugated microporous polymers. *Chem. Rev.* **120**, 2171–2214 (2020).
35. Li, Z. et al. Internalization pathways of anisotropic disc-shaped zeolite L nanocrystals with different surface properties in HeLa cancer cells. *Small* **9**, 1809–1820 (2013).
36. Wang, H., Pei, X., Kalmutzki, M. J., Yang, J. & Yaghi, O. M. Large cages of zeolitic imidazolate frameworks. *Acc. Chem. Res.* **55**, 707–721 (2022).
37. Diwakara, S. D. et al. Supramolecular reinforcement of a large-pore 2D covalent organic framework. *J. Am. Chem. Soc.* **144**, 2468–2473 (2022).
38. Zhou, Z.-B. et al. A facile, efficient, and general synthetic method to amide-linked covalent organic frameworks. *J. Am. Chem. Soc.* **144**, 1138–1143 (2022).
39. Mu, Z. et al. Covalent organic frameworks with record pore apertures. *J. Am. Chem. Soc.* **144**, 5145–5154 (2022).

40. Szczęśniak, B., Choma, J. & Jaroniec, M. Major advances in the development of ordered mesoporous materials. *Chem. Comm.* **56**, 7836–7848 (2020).
41. Davis, M. E. Ordered porous materials for emerging applications. *Nature* **417**, 813–821 (2002).
42. Corma, A. From microporous to mesoporous molecular sieve materials and their use in catalysis. *Chem. Rev.* **97**, 2373–2420 (1997).
43. Kresge, C. T., Leonowicz, M. E., Roth, W. J., Vartuli, J. C. & Beck, J. S. Ordered mesoporous molecular sieves synthesized by a liquid-crystal template mechanism. *Nature* **359**, 710–712 (1992).
44. Zhao, D. et al. Triblock copolymer syntheses of mesoporous silica with periodic 50 to 300 angstrom pores. *Science* **279**, 548–552 (1998).
45. Urata, C., Aoyama, Y., Tonegawa, A., Yamauchi, Y. & Kuroda, K. Dialysis process for the removal of surfactants to form colloidal mesoporous silica nanoparticles. *Chem. Comm.* **34**, 5094–5096 (2009).
46. Qiu, P., Ma, B., Hung, C.-T., Li, W. & Zhao, D. Spherical mesoporous materials from single to multilevel architectures. *Acc. Chem. Res.* **52**, 2928–2938 (2019).
47. Ariga, K., Vinu, A., Yamauchi, Y., Ji, Q. & Hill, J. P. Nanoarchitectonics for mesoporous materials. *Bull. Chem. Soc. Jpn* **85**, 1–32 (2011).
48. Zhao, D., Huo, Q., Feng, J., Chmelka, B. F. & Stucky, G. D. Nonionic triblock and star diblock copolymer and oligomeric surfactant syntheses of highly ordered, hydrothermally stable. mesoporous silica structures. *J. Am. Chem. Soc.* **120**, 6024 (1998).
49. Wang, X. et al. Synthesis of ordered mesoporous silica with tunable morphologies and pore sizes via a nonpolar solvent-assisted stöber method. *Chem. Mater.* **28**, 2356–2362 (2016).
50. Nugraha, A.S. et al. Symmetry-breaking plasmonic mesoporous gold nanoparticles with large pores. *Chem. Mater.* https://doi.org/10.1021/acs.chemmater.2c01125 (2022).
51. Chen, G., Bhadra, B. N., Sutrisno, L., Shrestha, L. K. & Ariga, K. Fullerene rosette: two-dimensional interactive nanoarchitectonics and selective vapor sensing. *Int. J. Mol. Sci.* **23**, 5454 (2022).
52. Peng, Y. et al. General surface-casting synthesis of mesoporous metal oxides with hollow structures and ultrahigh surface areas. *Chem. Mater.* **34**, 7042–7057 (2022).
53. Li, K., Yang, J. & Gu, J. Hierarchically porous MOFs synthesized by soft-template strategies. *Acc. Chem. Res.* **55**, 2235–2247 (2022).
54. Ma, W. et al. Morphology-controlled fabrication strategy of hollow mesoporous carbon spheres@f-Fe_2O_3 for microwave absorption and infrared stealth. *ACS Appl. Mater. Interfaces* **14**, 34985–34996 (2022).
55. Yan, Y. et al. Mesoporous nanoarchitectures for electrochemical energy conversion and storage. *Adv. Mater.* **32**, 44 (2020).
56. Ai, Y., Li, W. & Zhao, D. 2D mesoporous materials. *Nat. Soc. Rev.* **9**, 5 (2021).
57. Ryoo, R. et al. Rare-earth–platinum alloy nanoparticles in mesoporous zeolite for catalysis. *Nature* **585**, 221–224 (2020).
58. Jiang, Z. et al. Filling metal–organic framework mesopores with TiO_2 for CO_2 photoreduction. *Nature* **586**, 549–554 (2020).
59. Bennett, T. D., Coudert, F.-X., James, S. L. & Cooper, A. I. The changing state of porous materials. *Nat. Mater.* **20**, 1179–1187 (2021).
60. Liu, J. et al. A sensitive and specific nanosensor for monitoring extracellular potassium levels in the brain. *Nat. Nanotechnol.* **15**, 321–330 (2020).
61. Hunter, N. L., Rao, G. R. & Sherman, R. E. Flexibility in the FDA approach to orphan drug development. *Nat. Rev. Drug Discov.* **16**, 737–738 (2017).
62. Arora, S. et al. U.S. FDA drug approvals for gynecological malignancies: a decade in review. *Clin. Cancer Res* **28**, 1058–1071 (2022).
63. Chen, T. et al. Inhaled curcumin mesoporous polydopamine nanoparticles against radiation pneumonitis. *Acta Pharm. Sin. B* **12**, 2522–2532 (2021).
64. Wang, L. et al. Polycatechol-derived mesoporous polydopamine nanoparticles for combined ROS scavenging and gene interference therapy in inflammatory bowel disease. *ACS Appl. Mater. Interfaces* **14**, 19975–19987 (2022).
65. Li, T. et al. Surgical tumor-derived photothermal nanovaccine for personalized cancer therapy and prevention. *Nano Lett.* **22**, 3095–3103 (2022).
66. Alfieri, M. L., Weil, T., Ng, D. Y. W. & Ball, V. Polydopamine at biological interfaces. *Adv. Colloid Interface Sci.* **305**, 102689 (2022).
67. Jin, A., Wang, Y., Lin, K. & Jiang, L. Nanoparticles modified by polydopamine: Working as "drug" carriers. *Bioact. Mater.* **5**, 522–541 (2020).
68. Hu, H. et al. Mesoporous polydopamine-based multifunctional nanoparticles for enhanced cancer phototherapy. *J. Colloid Interf. Sci.* **612**, 246–260 (2022).
69. Wan, D., Yan, C. & Zhang, Q. Facile and rapid synthesis of hollow magnetic mesoporous polydopamine nanoflowers with tunable pore structures for lipase immobilization: green production of biodiesel. *Ind. Eng. Chem. Res.* **58**, 16358–16369 (2019).
70. Guan, Y., Yu, L. & Lou, X. W. Formation of asymmetric bowl-Like mesoporous particles via emulsion-induced interface anisotropic assembly. *J. Am. Chem. Soc.* **138**, 11306–11311 (2016).
71. Chen, J. et al. Localized degradation of neutrophil extracellular traps by photoregulated enzyme delivery for cancer immunotherapy and metastasis suppression. *ACS Nano* **16**, 2585–2597 (2022).
72. Liu, Y. et al. Remotely boosting hyaluronidase activity to normalize the hypoxic immunosuppressive tumor microenvironment for photothermal immunotherapy. *Biomaterials* **284**, 121516 (2022).
73. Li, T. et al. Sandwich-structured ordered mesoporous polydopamine/MXene hybrids as high-performance anodes for lithium-ion batteries. *ACS Appl. Mater. Interfaces* **12**, 14993–15001 (2020).
74. Tao, W. et al. Synthesis of multi-branched Au nanocomposites with distinct plasmon resonance in NIR-II window and controlled CRISPR-Cas9 delivery for synergistic gene-photothermal therapy. *Biomaterials* **287**, 121621 (2022).
75. Sasmal, H. S., Kumar Mahato, A., Majumder, P. & Banerjee, R. Landscaping covalent organic framework nanomorphologies. *J. Am. Chem. Soc.* **144**, 11482–11498 (2022).
76. Liu, X. et al. Recent advances in covalent organic frameworks (COFs) as a smart sensing material. *Chem. Soc. Rev.* **48**, 5266–5302 (2019).
77. Wang, H. et al. Recent progress in covalent organic framework thin films: fabrications, applications and perspectives. *Chem. Soc. Rev.* **48**, 488–516 (2019).
78. Wang, H. et al. Covalent organic framework photocatalysts: structures and applications. *Chem. Soc. Rev.* **49**, 4135 (2020).
79. Liao, C. & Liu, S. Tuning the physicochemical properties of reticular covalent organic frameworks (COFs) for biomedical applications. *J. Mater. Chem. B* **9**, 6116–6128 (2021).
80. Mal, A., Ding, H., Li, M., Li, W. & Wang, C. Covalent organic frameworks with nanopores for biological applications: a review. *ACS Appl. Nano Mater.* https://doi.org/10.1021/acsanm.2c01517 (2022).
81. Esrafili, A., Wagner, A., Inamdar, S. & Acharya, A. P. Covalent organic frameworks for biomedical applications. *Adv. Healthc. Mater.* **10**, 2002090 (2021).
82. Bhunia, S., Deo, K. A. & Gaharwar, A. K. 2D covalent organic frameworks for biomedical applications. *Adv. Funct. Mater.* **30**, 2002046 (2020).
83. Dutta, D., Wang, J., Li, X., Zhou, Q. & Ge, Z. Covalent organic framework nanocarriers of singlet oxygen for oxygen-independent concurrent photothermal/photodynamic therapy to ablate hypoxic tumors. *Small* **18**, 2202369 (2022).
84. Bhunia, S., Saha, P., Moitra, P., Addicoat, M. A. & Bhattacharya, S. Efficacious and sustained release of an anticancer drug mitoxantrone from new covalent organic frameworks using protein corona. *Chem. Sci.* **13**, 7920 (2022).
85. Bai, L. et al. Nanoscale covalent organic frameworks as smart carriers for drug delivery. *Chem. Commun.* **52**, 4128–4131 (2016).
86. Zhou, Y. et al. Double-activation of mitochondrial permeability transition pore opening via calcium overload and reactive oxygen species for cancer therapy. *J. Nanobiotechnology* **20**, 188 (2022).
87. Song, S. et al. Donor-acceptor structured photothermal COFs for enhanced starvation therapy. *Chem. Eng. J.* **442**, 135963 (2022).
88. Kankala, R. K., Han, Y.-H., Xia, H.-Y., Wang, S.-B. & Chen, A.-Z. Nanoarchitectured prototypes of mesoporous silica nanoparticles for innovative biomedical applications. *J. Nanobiotechnology* **20**, 126 (2022).
89. Yang, P., Gai, S. & Lin, J. Functionalized mesoporous silica materials for controlled drug delivery. *Chem. Soc. Rev.* **41**, 3679–3698 (2012).
90. Morales, V. et al. New drug-structure-directing agent concept: inherent pharmacological activity combined with templating solid and hollow-shell mesostructured silica nanoparticles. *Adv. Funct. Mater.* **26**, 7291–7303 (2016).
91. Suteewong, T. et al. Highly aminated mesoporous silica nanoparticles with cubic pore structure. *J. Am. Chem. Soc.* **133**, 172–175 (2011).
92. Hao, Z., Li, S., Sun, J., Li, S. & Zhang, F. Efficient visible-light-driven depolymerization of oxidized lignin to aromatics catalyzed by an iridium complex immobilized on mesocellular silica foams. *Appl. Catal. B Environ.* **237**, 366–372 (2018).
93. Vafaeezadeh, M. et al. Janus bifunctional periodic mesoporous organosilica. *Chem. Commun.* **58**, 112–115 (2022).
94. Li, C. et al. Phosphotungstate-functionalized mesoporous janus silica nanosheets for reaction-controlled pickering interfacial catalysis. *ACS Sustain. Chem. Eng.* **9**, 13501–13513 (2021).

95. Gao, F. et al. Flower-like mesoporous silica: a bifunctionalized catalyst for rhodium-catalyzed asymmetric transfer hydrogenation of aromatic ketones in aqueous medium. *Green. Chem.* **15**, 2208–2214 (2013).
96. Singh, A. K. et al. Lipid-coated MCM-41 mesoporous silica nanoparticles loaded with berberine improved inhibition of acetylcholine esterase and amyloid formation. *ACS Biomater. Sci. Eng.* **7**, 3737–3753 (2021).
97. Febriyanti, E. et al. Thermodynamic picture of phase segregation during the formation of bicontinuous concentric lamellar (bcl) silica. *Langmuir* **38**, 1368–1379 (2022).
98. Sun, L., Zhang, X., Zheng, C., Wu, Z. & Li, C. A pH gated, glucose-sensitive nanoparticle based on worm-Like mesoporous silica for controlled insulin release. *J. Phys. Chem. B* **117**, 3852–3860 (2013).
99. Qiao, S. Z. et al. Disulfide-bridged organosilica frameworks: designed, synthesis, redox-triggered biodegradation, and nanobiomedical applications. *Adv. Funct. Mater.* **28**, 1707325 (2018).
100. He, Q., Zhang, Z., Gao, F., Li, Y. & Shi, J. In vivo biodistribution and urinary excretion of mesoporous silica nanoparticles: effects of particle size and PEGylation. *Small* **7**, 271–280 (2011).
101. He, Q., Zhang, Z., Gao, Y., Shi, J. & Li, Y. Intracellular localization and cytotoxicity of spherical mesoporous silica nano- and microparticles. *Small* **5**, 2722–2729 (2009).
102. Živojević, K. et al. Advanced mesoporous silica nanocarriers in cancer theranostics and gene editing applications. *J. Control. Release* **337**, 193–211 (2021).
103. Ye, Z. et al. Construction of nanomotors with replaceable engines by supramolecular machine-based host–guest assembly and disassembly. *J. Am. Chem. Soc.* **143**, 15063–15072 (2021).
104. Tang, F., Li, L. & Chen, D. Mesoporous silica nanoparticles: synthesis, biocompatibility and drug delivery. *Adv. Mater.* **24**, 1504–1534 (2012).
105. Slapak, E. J., Mandili, M. E., Bijslma, M. F. & Spek, C. A. Mesoporous silica nanoparticle-based drug delivery systems for the treatment of pancreatic cancer: a systematic literature overview. *Pharmaceutics* **14**, 2 (2022).
106. Wang, J. et al. Facile and controllable synthesis of the renal-clearable "luminous pearls" for in vivo afterglow/magnetic resonance imaging. *ACS Nano* **16**, 462–472 (2022).
107. Angiolini, L., Valetti, S., Cohen, B., Feiler, A. & Douhal, A. Fluorescence imaging of antibiotic clofazimine encapsulated within mesoporous silica particle carriers: relevance to drug delivery and the effect on its release kinetics. *Phys. Chem. Chem. Phys.* **20**, 11899 (2018).
108. Zhang, H. et al. A soft–hard template approach towards hollow mesoporous silica nanoparticles with rough surfaces for controlled drug delivery and protein adsorption. *J. Mater. Chem. B* **3**, 6480 (2015).
109. Yu, L. et al. Ultrasmall mesoporous organosilica nanoparticles: morphology modulations and redox-responsive biodegradability for tumor-specific drug delivery. *Biomaterials* **161**, 292–305 (2018).
110. Cho, E. B., Choi, E., Yang, S. & Jaroinec, M. Hollow mesoporous organosilica nanospheres templated with flower-like micelles of pentablock copolymers. *J. Colloid Interface Sci.* **528**, 124–134 (2018).
111. Wu, M. et al. Large pore-sized hollow mesoporous organosilica for redox-responsive gene delivery and synergistic cancer chemotherapy. *Adv. Mater.* **28**, 1963 (2016).
112. Luo, L., Wang, X., Liao, Y.-P., Chang, C. H. & Nel, A. E. Nanocarrier coformulation for delivery of a TLR7 agonist plus an immunogenic cell death stimulus triggers effective pancreatic cancer chemo-immunotherapy. *ACS Nano* **16**, 13168–13182 (2022).
113. Escriche-Navarro, B. et al. Mesoporous silica materials as an emerging tool for cancer immunotherapy. *Adv. Sci.* https://doi.org/10.1002/advs.202200756 (2022).
114. Abbaraju, L. et al. Asymmetric silica nanoparticles with tunable head–tail structures enhance hemocompatibility and maturation of immune cells. *J. Am. Chem. Soc.* **139**, 6321 (2017).
115. Zhang, Y., Zhu, J., Huang, G., Zhu, J. & He, D. Potential applications of multifunctional mesoporous carbon nanoplatform for tumor microenvironment improving by combined chemo-/phototherapy. *Carbon* **163**, 128–136 (2020).
116. Gisbert-Garzarán, M. et al. Engineered pH-responsive mesoporous carbon nanoparticles for drug delivery. *ACS Appl. Mater. Interfaces* **12**, 14946–14957 (2020).
117. Jeong, J. et al. Color-tunable photoluminescent fullerene nanoparticles. *Adv. Mater.* **24**, 1999–2003 (2012).
118. Hirao, T., Iwabe, Y., Fujii, N. & Haino, T. Helically organized fullerene array in a supramolecular polymer main chain. *J. Am. Chem. Soc.* **143**, 4339–4345 (2021).
119. Krishnan, V. et al. Vortex-aligned fullerene nanowhiskers as a scaffold for orienting cell growth. *ACS Appl. Mater. Interfaces* **7**, 15667–15673 (2015).
120. Minami, K., Song, J., Shrestha, L. K. & Ariga, K. Nanoarchitectonics for fullerene biology. *Appl. Mater. Today* **23**, 100989 (2021).
121. Miyazawa, K. et al. Fullerene nanowhiskers and related fullerene nanomaterials. *J. Phys. Conf. Ser.* **159**, 012007 (2009).
122. Miyazawa, K. et al. Structural characterization of C_{60} nanowhiskers formed by the liquid/liquid interfacial precipitation method. *Surf. Interface Anal.* **35**, 117–120 (2003).
123. Shrestha, L. K. et al. Nanoporous carbon tubes from fullerene crystals as the π-electron carbon source. *Angew. Chem. Int. Ed.* **54**, 951–955 (2015).
124. Schüßlbauer, C. M. et al. Exploring the threshold between fullerenes and nanotubes: characterizing isomerically pure, empty-caged, and tubular fullerenes D5h-C_{90} and D5d-C_{100}. *J. Am. Chem. Soc.* **144**, 10825–10829 (2022).
125. Wakahara, T., Nemoto, Y., Xu, M., Miyazawa, K. & Fujita, D. Preparation of endohedral metallofullerene nanowhiskers and nanosheets. *Carbon* **48**, 3359–3363 (2010).
126. Hou, L. et al. Synthesis of a monolayer fullerene network. *Nature* **606**, 507–510 (2022).
127. Bairi, P. et al. Hierarchically structured fullerene C_{70} cube for sensing volatile aromatic solvent vapors. *ACS Nano* **10**, 6631–6637 (2016).
128. Bairi, P. et al. Mesoporous fullerene C_{70} cubes with highly crystalline frameworks and unusually enhanced photoluminescence properties. *Mater. Horiz.* **5**, 285–290 (2018).
129. Wei, Z., Song, J., Ma, R., Ariga, K. & Shrestha, L. K. Self-assembled corn-husk-shaped fullerene crystals as excellent acid vapor sensors. *Chemosensors* **10**, 16 (2022).
130. Minami, K. et al. Highly ordered 1D fullerene crystals for concurrent control of macroscopic cellular orientation and differentiation toward large-scale tissue engineering. *Adv. Mater.* **27**, 4020–4026 (2015).
131. Hsieh, F.-Y., Shrestha, L. K., Ariga, K. & Hsu, S. Neural differentiation on aligned fullerene C_{60} nanowhiskers. *Chem. Commun.* **53**, 11024–11027 (2017).
132. Song, J. et al. Large-area aligned fullerene nanocrystal scaffolds as culture substrates for enhancing mesenchymal stem cell self-renewal and multipotency. *ACS Appl. Nano Mater.* **3**, 6497–6506 (2020).
133. Deng, X., Chen, K. & Tüysüz, H. Protocol for the nanocasting method: preparation of ordered mesoporous metal oxides. *Chem. Mater.* **29**, 40–52 (2017).
134. Ren, Y., Ma, Z. & Bruce, P. G. Ordered mesoporous metal oxides: synthesis and applications. *Chem. Soc. Rev.* **41**, 4909–4927 (2012).
135. Yu, C. et al. Aza-BODIPY probe-decorated mesoporous black TiO_2 nanoplatform for the highly efficient synergistic phototherapy. *ACS Appl. Mater. Interfaces* **12**, 41071–41078 (2020).
136. Wang, S. et al. Triple stimuli-responsive ZnO quantum dots-conjugated hollow mesoporous carbon nanoplatform for NIR-induced dual model antitumor therapy. *Biomaterials* **559**, 51–64 (2020).
137. Wu, Y. et al. Black phosphorus quantum dots encapsulated biodegradable hollow mesoporous MnO_2: dual-modality cancer imaging and synergistic chemo-phototherapy. *Adv. Funct. Mater.* **31**, 2104643 (2021).
138. Yi, T. et al. Hybrid mesoporous MnO_2-upconversion nanoparticles for image-guided lung cancer spinal metastasis therapy. *ACS Appl. Mater. Interfaces* **14**, 18031–18042 (2022).
139. Li, Y., Du, L., Li, F., Deng, Z. & Zeng, S. Intelligent nanotransducer for deep-tumor hypoxia modulation and enhanced dual-photosensitizer photodynamic therapy. *ACS Appl. Mater. Interfaces* **14**, 14944–14952 (2022).
140. Zuo, W. et al. Macrophage-mimic hollow mesoporous Fe-based nanocatalysts for self-amplified chemodynamic therapy and metastasis inhibition via tumor microenvironment remodeling. *ACS Appl. Mater. Interfaces* **14**, 5053–5065 (2022).
141. Guo, Z.-Y. et al. Magnetic nanospheres encapsulated by mesoporous copper oxide shell for selective isolation of hemoglobin. *ACS Appl. Mater. Interfaces* **8**, 29734–29741 (2016).
142. Behera, P., Subudhi, S., Tripathy, S. P. & Parida, K. MOF derived nano-materials: A recent progress in strategic fabrication, characterization and mechanistic insight towards divergent photocatalytic applications. *Coord. Chem. Rev.* **456**, 214392 (2022).

143. Yang, W., Feng, J. & Zhang, H. Facile and rapid fabrication of nanostructured lanthanide coordination polymers as selective luminescent probes in aqueous solution. *J. Mater. Chem.* **22**, 6819–6823 (2012).
144. Horcajada, P. et al. Colloidal route for preparing optical thin films of nanoporous metal–organic frameworks. *Adv. Mater.* **21**, 1931–1935 (2009).
145. Rieter, W. J., Taylor, K. M. L., An, H., Lin, W. & Lin, W. Nanoscale metal−organic frameworks as potential multimodal contrast enhancing agents. *J. Am. Chem. Soc.* **128**, 9024–9025 (2006).
146. Duan, D. et al. Size-controlled synthesis of drug-loaded zeolitic imidazolate framework in aqueous solution and size effect on their cancer theranostics in vivo. *ACS Appl. Mater. Interfaces* **10**, 42165–42174 (2018).
147. Li, S., Tan, L. & Meng, X. Nanoscale metal-organic frameworks: synthesis, biocompatibility, imaging applications, and thermal and dynamic therapy of tumors. *Adv. Funct. Mater.* **30**, 1908924 (2020).
148. Crosby, D. et al. Early detection of cancer. *Science* **375**, eaay9040 (2022).
149. Kim, M. et al. A protein interaction landscape of breast cancer. *Science* **374**, eabf3066 (2021).
150. Xing, P. & Zhao, Y. Supramolecular vesicles for stimulus-responsive drug delivery. *Small Methods* **2**, 1700364 (2018).
151. Rolver, M. G. & Pedersen, S. F. Putting warburg to work: how imaging of tumour acidosis could help predict metastatic potential in breast cancer. *Br. J. Cancer* **124**, 1–2 (2021).
152. Woodford, M. R. et al. The tumor suppressor folliculin inhibits lactate dehydrogenase A and regulates the Warburg effect. *Nat. Struct. Mol. Biol.* **28**, 662–670 (2021).
153. Yan, Y. et al. Dissecting extracellular and intracellular distribution of nanoparticles and their contribution to therapeutic response by monochromatic ratiometric imaging. *Nat. Commun.* **13**, 2004 (2022).
154. Huang, X., Wu, S. & Du, X. Gated mesoporous carbon nanoparticles as drug delivery system for stimuli-responsive controlled release. *Carbon* **101**, 135–142 (2016).
155. Jiao, J. et al. Redox and pH dual-responsive PEG and chitosan-conjugated hollow mesoporous silica for controlled drug release. *Mater. Sci. Eng. C.* **67**, 26–33 (2016).
156. Zou, Z. et al. Natural gelatin capped mesoporous silica nanoparticles for intracellular acid-triggered drug delivery. *Langmuir* **29**, 12804–12810 (2013).
157. Butler, K. S. et al. Protocells: modular mesoporous silica nanoparticle-supported lipid bilayers for drug delivery. *Small* **12**, 2173–2185 (2016).
158. Durfee, P. N. et al. Mesoporous silica nanoparticle-supported lipid bilayers (protocells) for active targeting and delivery to individual leukemia cells. *ACS Nano* **10**, 8325–8345 (2016).
159. Niedermayer, S. et al. Multifunctional polymer-capped mesoporous silica nanoparticles for pH-responsive targeted drug delivery. *Nanoscale* **7**, 7953–7964 (2015).
160. Yang, K. N. et al. pH-responsive mesoporous silica nanoparticles employed in controlled drug delivery systems for cancer treatment. *Cancer Biol. Med.* **11**, 34–43 (2014).
161. Xing, L., Zheng, H., Cao, Y. & Che, S. Coordination polymer coated mesoporous silica nanoparticles for pH-responsive drug release. *Adv. Mater.* **24**, 6433–6437 (2012).
162. Cai, Y., Deng, T., Pan, Y. & Zink, J. I. Use of ferritin capped mesoporous silica nanoparticles for redox and pH triggered drug release in vitro and in vivo. *Adv. Funct. Mater.* **30**, 2002043 (2020).
163. Feng, W. et al. Polyelectrolyte multilayer functionalized mesoporous silica nanoparticles for pH-responsive drug delivery: layer thickness-dependent release profiles and biocompatibility. *J. Mater. Chem. B* **1**, 5886–5898 (2013).
164. Li, Q.-L. et al. Mesoporous silica nanoparticles coated by layer-by-layer self-assembly using cucurbit[7]uril for in vitro and in vivo anticancer drug release. *Chem. Mater.* **26**, 6418–6431 (2014).
165. Dai, L. et al. Multifunctional metal-organic framework-based nanoreactor for starvation/oxidation improved indoleamine 2,3-dioxygenase-blockade tumor immunotherapy. *Nat. Comm.* **13**, 2688 (2012).
166. Zhuo, S. et al. pH-sensitive biomaterials for drug delivery. *Molecules* **25**, 5649 (2020).
167. Meng, H. et al. Autonomous in vitro anticancer drug release from mesoporous silica nanoparticles by pH-sensitive nanovalves. *J. Am. Chem. Soc.* **132**, 12690–12697 (2010).
168. William, C. S. et al. Irreversible inhibition of cytosolic thioredoxin reductase 1 as a mechanistic basis for anticancer therapy. *Sci. Transl. Med.* **10**, eaaf7444 (2018).
169. Niu, B. et al. Application of glutathione depletion in cancer therapy: enhanced ROS-based therapy, ferroptosis, and chemotherapy. *Biomaterials* **277**, 121110 (2021).
170. Huo, M., Yuan, J., Tao, L. & Wei, Y. Redox-responsive polymers for drug delivery: from molecular design to applications. *Polym. Chem.* **5**, 1519–1528 (2014).
171. Zhang, Y. et al. Dendritic mesoporous silica nanoparticle-tuned high-affinity MnO_2 nanozyme for multisignal GSH sensing and target cancer cell detection. *ACS Sus. Chem. Eng.* **10**, 5911–5921 (2022).
172. Moghaddam, S. P., Saikia, J., Yazdimamaghani, M. & Ghandehari, H. Redox-responsive polysulfide-based biodegradable organosilica nanoparticles for delivery of bioactive agents. *ACS Appl. Mater. Interfaces* **9**, 21133 (2017).
173. Lei, L. et al. Structure inversion-bridged sequential amino acid metabolism disturbance potentiates photodynamic-evoked immunotherapy. *Adv. Funct. Mater.* **32**, 2103394 (2022).
174. Hadipour Moghaddam, S. P., Yazdimamaghani, M. & Ghandehari, H. Glutathione-sensitive hollow mesoporous silica nanoparticles for controlled drug delivery. *J. Control. Release* **282**, 62–75 (2018).
175. Wu, M. et al. Focused ultrasound-augmented delivery of biodegradable multifunctional nanoplatforms for imaging-guided brain tumor treatment. *Adv. Sci.* **5**, 1700474 (2018).
176. Mao, D. et al. AIEgen-coupled upconversion nanoparticles eradicate solid tumors through dual-mode ROS activation. *Sci. Adv.* **6**, eabb2712 (2020).
177. Perillo, B. et al. ROS in cancer therapy: the bright side of the moon. *Exp. Mol. Med.* **52**, 192–203 (2020).
178. Xue, C.-C. et al. Tumor microenvironment-activatable Fe-doxorubicin preloaded amorphous CaCO3 nanoformulation triggers ferroptosis in target tumor cells. *Sci. Adv.* **6**, eaax1346 (2020).
179. Shehan, J. et al. Biomarkers for glioblastoma: MMP2 and NGAL. *J. Clin. Oncol.* **34**, e13516–e13516 (2016).
180. Chen, Y., Ma, H., Wang, W. & Zhang, M. A size-tunable nanoplatform: enhanced MMP2-activated chemo-photodynamic immunotherapy based on biodegradable mesoporous silica nanoparticles. *Biomater. Sci.* **9**, 917–929 (2021).
181. Kim, Y.-J., Ebara, M. & Aoyagi, T. A smart hyperthermia nanofiber with switchable drug release for inducing cancer apoptosis. *Adv. Funct. Mater.* **23**, 5753–5761 (2013).
182. Zhang, Y. et al. A near-infrared photo-switched microRNA amplifier for precise photodynamic therapy of early-stage cancers. *Angew. Chem. Int. Ed.* **59**, 21454–21459 (2020).
183. Lee, H. P. & Gaharwar, A. K. Light-responsive inorganic biomaterials for biomedical applications. *Adv. Sci.* **7**, 2000863 (2020).
184. Chen, G. et al. Advanced near-infrared light for monitoring and modulating the spatiotemporal dynamics of cell functions in living systems. *Adv. Sci.* **7**, 1903783 (2020).
185. Zheng, S. et al. Biocompatible nanomotors as active diagnostic imaging agents for enhanced magnetic resonance imaging of tumor tissues in vivo. *Adv. Funct. Mater.* **31**, 2100936 (2021).
186. Nasseri, B. et al. Nanomaterials for photothermal and photodynamic cancer therapy. *Appl. Phys. Rev.* **9**, 011317 (2022).
187. Xiong, J. et al. Engineering a theranostic platform for synergistic hypoxia-responsive photodynamic therapy and chemotherapy. *Matter* **5**, 1502–1519 (2022).
188. Peng, C. et al. Hollow mesoporous tantalum oxide based nanospheres for triple sensitization of radiotherapy. *ACS Appl. Mater. Interfaces* **12**, 5520–5530 (2020).
189. Chen, Y. et al. Degradable mesoporous semimetal antimony nanospheres for near-infrared II multimodal theranostics. *Nat. Comm.* **13**, 539 (2022).
190. Wu, X. et al. Chemo-phototherapy with carfilzomib-encapsulated TiN nanoshells suppressing tumor growth and lymphatic metastasis. *Small* **18**, 2200522 (2022).
191. Luo, T. et al. Dimensional reduction enhances photodynamic therapy of metal–organic nanophotosensitizers. *J. Am. Chem. Soc.* **144**, 5241–5246 (2022).
192. Xu, X.-L. et al. Sialic acid-modified mesoporous polydopamine induces tumor vessel normalization to enhance photodynamic therapy by inhibiting VE-cadherin internalization. *Chem. Eng. J.* **414**, 128743 (2021).
193. Han, H., Lee, H., Kim, K. & Kim, H. Effect of high intensity focused ultrasound (HIFU) in conjunction with a nanomedicines-microbubble complex for enhanced drug delivery. *J. Control. Release* **266**, 75–86 (2017).

194. Lin, F.-C., Xie, Y., Deng, T. & Zink, J. I. Magnetism, ultrasound, and light-stimulated mesoporous silica nanocarriers for theranostics and beyond. *J. Am. Chem. Soc.* **143**, 6025–6036 (2021).
195. Xu, Z., Liu, H., Tian, H. & Yan, F. Real-time imaging tracking of engineered macrophages as ultrasound-triggered cell bombs for cancer treatment. *Adv. Funct. Mater.* **30**, 1910304 (2020).
196. Wang, M. et al. A multifunctional nanovaccine based on l-arginine-loaded black mesoporous titania: ultrasound-triggered synergistic cancer sonodynamic therapy/gas therapy/immunotherapy with remarkably enhanced efficacy. *Small* **17**, e2005728 (2021).
197. Qiao, L. et al. Laccase-mediated formation of mesoporous silica nanoparticle based redox stimuli-responsive hybrid nanogels as a multifunctional nanotheranostic agent. *Nanoscale* **39**, 17241–17249 (2016).
198. Feng, L. et al. Near-infrared upconversion mesoporous tin oxide biophotocatalyst for H_2O_2-activatable O_2-generating magnetic targeting synergetic treatment. *ACS Appl. Mater. Interfaces* **12**, 41047–41061 (2020).
199. Chen, W., Cheng, C.-A. & Zink, J. I. Spatial, temporal, and dose control of drug delivery using noninvasive magnetic stimulation. *ACS Nano* **13**, 1292–1308 (2019).
200. Feng, Y. et al. Magnetic manganese oxide sweetgum-ball nanospheres with large mesopores regulate tumor microenvironments for enhanced tumor nanotheranostics. *ACS Appl. Mater. Interfaces* **11**, 37461–37470 (2019).
201. Xuan, M. et al. Magnetic mesoporous silica nanoparticles cloaked by red blood cell membranes: applications in cancer therapy. *Angew. Chem. Int. Ed.* **57**, 6049–6053 (2018).
202. Li, Y. & Shi, J. Hollow-structured mesoporous materials: chemical synthesis, functionalization and applications. *Adv. Mater.* **26**, 3176–3205 (2014).
203. Rahikkala, A. et al. Mesoporous silica nanoparticles for targeted and stimuli-responsive delivery of chemotherapeutics: a review. *Adv. Biosyst.* **2**, 1800020 (2018).
204. Vallet-Regí, M., Balas, F., Colilla, M. & Manzano, M. Bone-regenerative bioceramic implants with drug and protein controlled delivery capability. *Prog. Solid. State Chem.* **36**, 163–191 (2008).
205. Yang, B., Chen, Y. & Shi, J. Mesoporous silica/organosilica nanoparticles: synthesis, biological effect and biomedical application. *Mat. Sci. Eng. R.* **137**, 66–105 (2019).
206. Nagy, J. A., Chang, S. H., Dvorak, A. M. & Dvorak, H. F. Why are tumour blood vessels abnormal and why is it important to know? *Br. J. Cancer* **100**, 865–869 (2009).
207. Yu, W., Liu, R., Zhou, Y. & Gao, H. Size-tunable strategies for a tumor targeted drug delivery system. *ACS Cent. Sci.* **6**, 100–116 (2020).
208. Kim, J. et al. Programmed nanoparticle-loaded nanoparticles for deep-penetrating 3D cancer therapy. *Adv. Mater.* **30**, 1707557 (2018).
209. Rosenblum, D., Joshi, N., Tao, W., Karp, J. M. & Peer, D. Progress and challenges towards targeted delivery of cancer therapeutics. *Nat. Comm.* **9**, 1410 (2018).
210. Deng, Z. et al. Hollow chitosan-silica nanospheres as pH-sensitive targeted delivery carriers in breast cancer therapy. *Biomaterials* **32**, 4976–4986 (2011).
211. Allen, T. M. Ligand-targeted therapeutics in anticancer therapy. *Nat. Rev. Cancer* **2**, 750–763 (2002).
212. Li, Q. et al. Aptamers: a novel targeted theranostic platform for pancreatic ductal adenocarcinoma. *Radiat. Oncol.* **15**, 189 (2020).
213. Chen, C., Zhou, Y., Chen, C., Zhu, S. & Yan, X. Quantification of available ligand density on the surface of targeted liposomal nanomedicines at the single-particle level. *ACS Nano* **16**, 6886–6897 (2022).
214. Bai, H. et al. Cyclodextrin-based host-guest complexes loaded with regorafenib for colorectal cancer treatment. *Nat. Commun.* **12**, 759 (2021).
215. Nakamura, T. et al. Extrahepatic targeting of lipid nanoparticles in vivo with intracellular targeting for future nanomedicines. *Adv. Drug Deliv. Rev.* **188**, 114417 (2022).
216. Li, W.-N., Zhang, S.-J., Feng, J.-Q. & Jin, W.-L. Repurposing vitamin C for vancer treatment: focus on targeting the tumor microenvironment. *Cancers* **14**, 2608 (2022).
217. Tsai, C.-P., Chen, C.-Y., Hung, Y., Chang, F.-H. & Mou, C.-Y. Monoclonal antibody-functionalized mesoporous silica nanoparticles (MSN) for selective targeting breast cancer cells. *J. Mater. Chem.* **19**, 5737–5743 (2009).
218. Wang, Y. et al. pH/H_2O_2 dual-responsive chiral mesoporous silica nanorods coated with a biocompatible active targeting ligand for cancer therapy. *ACS Appl. Mater. Interfaces* **13**, 35397–35409 (2021).
219. Zhao, S. et al. In situ synthesis of fluorescent mesoporous silica-carbon dot nanohybrids featuring folate receptor-overexpressing cancer cell targeting and drug delivery. *Nano-Micro Lett.* **11**, 32 (2019).
220. Sagir, T. et al. Folic acid conjugated PAMAM-modified mesoporous silica-coated superparamagnetic iron oxide nanoparticles for potential cancer therapy. *J. Coll. Interface Sci.* **625**, 711–721 (2022).
221. Pan, L. et al. Nuclear-targeted drug delivery of TAT peptide-conjugated monodisperse mesoporous silica nanoparticles. *J. Am. Chem. Soc.* **134**, 5722–5725 (2012).
222. Park, I.-S. et al. Multifunctional synthetic nano-chaperone for peptide folding and intracellular delivery. *Nat. Comm.* **13**, 4568 (2022).
223. Li, S., Xing, R., Hest, J. C. M. & Yan, X. Peptide-based supramolecular assembly drugs toward cancer theranostics. *Expert Opin. Drug. Deliv.* **19**, 847–860 (2022).
224. Tan, A., Eskandar, N. G., Rao, S. & Prestidge, C. A. First in man bioavailability and tolerability studies of a silica–lipid hybrid (Lipoceramic) formulation: a Phase I study with ibuprofen. *Drug Deliv. Transl. Res.* **4**, 212–221 (2014).
225. Kharlamov, A. N. et al. Silica-gold nanoparticles for atheroprotective management of plaques: results of the NANOM-FIM trial. *Nanoscale* **7**, 8003–8015 (2015).
226. Kharlamov, A. N. et al. Plasmonic photothermal therapy of atherosclerosis with nanoparticles: long-term outcomes and safety in NANOM-FIM trial. *Future Cardiol.* **13**, 345–363 (2017).
227. Rastinehad Ardeshir, R. et al. Gold nanoshell-localized photothermal ablation of prostate tumors in a clinical pilot device study. *Proc. Natl Acad. Sci. U. S. A.* **116**, 18590–18596 (2019).
228. Janjua, T. I., Cao, Y., Yu, C. & Popat, A. Clinical translation of silica nanoparticles. *Nat. Rev. Mater.* **6**, 1072–1074 (2021).
229. Zanoni, D. K. et al. Use of ultrasmall core-shell fluorescent silica nanoparticles for image-guided sentinel lymph node biopsy in head and neck melanoma: a nonrandomized clinical trial. *JAMA Netw. Open* **4**, e211936 (2021).
230. Phillips, E. et al. Clinical translation of an ultrasmall inorganic optical-PET imaging nanoparticle probe. *Sci. Transl. Med.* **6**, 260ra149 (2014).
231. Zhang, K. et al. Complete tumor response following intratumoral 32P biosilicon on human hepatocellular and pancreatic carcinoma xenografts in nude mice. *Clin. Cancer Res* **11**, 7532–7537 (2005).
232. Croissant, J. G., Butler, K. S., Zink, J. I. & Brinker, C. J. Synthetic amorphous silica nanoparticles: toxicity, biomedical and environmental implications. *Nat. Rev. Mater.* **5**, 886–909 (2020).
233. Ge, C. et al. The contributions of metal impurities and tube structure to the toxicity of carbon nanotube materials. *NPG Asia Mater.* **4**, e32 (2012).
234. Mitchell, M. J. et al. Engineering precision nanoparticles for drug delivery. *Nat. Rev. Drug Discov.* **20**, 101–124 (2021).
235. Aono, M. & Ariga, K. The way to nanoarchitectonics and the way of nanoarchitectonics. *Adv. Mater.* **28**, 989–992 (2016).
236. Chaikittisilp, W., Yamauchi, Y. & Ariga, K. Material evolution with nanotechnology, nanoarchitectonics, and materials informatics: What will be the next paradigm shift in nanoporous materials. *Adv. Mater.* **34**, 2107212 (2022).